Existence of travelling wave solutions for a model of tumour invasion

K. Harley[†], P. van Heijster[†], R. Marangell[‡], G. J. Pettet[†], and M. Wechselberger[‡]

Abstract. The existence of travelling wave solutions to a haptotaxis dominated model is analysed. A version of this model has been derived in Perumpanani *et al.* (1999) to describe tumour invasion, where diffusion is neglected as it is assumed to play only a small role in the cell migration. By instead allowing diffusion to be small, we reformulate the model as a singular perturbation problem, which can then be analysed using geometric singular perturbation theory. We prove the existence of three types of physically realistic travelling wave solutions in the case of small diffusion. These solutions reduce to the no diffusion solutions in the singular limit as diffusion as is taken to zero. A fourth travelling wave solution is also shown to exist, but that is physically unrealistic as it has a component with negative cell population. The numerical stability, in particular the wavespeed of the travelling wave solutions is also discussed.

Key words. advection-reaction-diffusion systems, canards, singularly perturbed systems, travelling wave solutions

AMS subject classifications. 34C37, 34E17, 35C07, 35L67, 92C17

1. Introduction.

1.1. Travelling waves in cell migration.
Cell migration has been studied by both biologists and mathematicians for years, see for example [4, 28] and references within. It is important in a variety of contexts including wound healing, cancer (or other tumour) growth, and embryonic growth and development. Travelling wave solutions arising from continuum mathematical models to describe various modes of cell migration (purely diffusive, purely advective or a combination of both) are of particular interest. As well as the mode of migration, the speed of the travelling wave solutions is of interest, as this corresponds to the rate of invasion of cells.

One of the most famous examples of a model exhibiting travelling wave solutions is the Fisher–KPP equation [8, 16]. This model has been extensively studied and is an example of travelling wave solutions arising from a purely diffusive flux term. Another class of models known to exhibit travelling waves are the Keller–Segel type models [14, 15]. These models describe cell migration resulting from a combined diffusive and advective flux term. Advective motion (or advection) is the preferential motion of cells in a particular direction. This could be due to the flow of a fluid they are suspended in, or a response to a chemical gradient, for example. In all these examples, the observed travelling wave solutions are smooth. However, if the effect of diffusion on cell migration is reduced so that the balance between diffusive and advective migration shifts towards purely advective, the fronts of the travelling wave solutions can steepen and become *shock-like*. Note that true shocks or discontinuities will not be observed if even a small amount of diffusion is present.

True shocks, or solutions containing actual discontinuities arise from models with a purely

[†]Mathematical Sciences School, Queensland University of Technology, Brisbane, QLD 4000 Australia
[‡]School of Mathematics and Statistics, University of Sydney, Sydney, NSW 2006 Australia

advective flux term. This type of flux term can be used to model cell migration if, for example, cells are migrating in response to a gradient in a chemical that is bound to some surface. The bound chemical reduces the amount of *random* motion of the cells considerably and hence diffusive-like motion is minimal or non-existent. In these types of models, travelling wave solutions are still observed, and furthermore, the shock-like behaviour observed in the low diffusion case can develop into actual shocks. It is the low diffusion, high advection limit of cell migration that we are interested in.

1.2. Shock-fronted travelling waves. One approach for analysing shock-fronted travelling waves is based on dynamical systems theory, with the aim to identify travelling wave solutions of partial differential equation (PDE) systems as heteroclinic orbits of an associated ordinary differential equation (ODE) system. By applying such an approach to models of purely chemotactically (advectively) driven growth processes, systems of two-species, coupled, ODEs of the form

$$\frac{\mathrm{d}u}{\mathrm{d}z} = R(u, w),$$
$$P(u, w)\frac{\mathrm{d}w}{\mathrm{d}z} = Q(u, w) \tag{1.1}$$

were uncovered [30, 31]. Systems of first order differential equations such as these can be studied using methods from dynamical systems theory (see for example [12, 27]), where solution trajectories are analysed in the (u, w)-phase plane. However, due to the term premultiplying the left-hand side, this type of ODE system leads to singularities in the phase plane for $P(u, w) = 0$ and $Q(u, w) \neq 0$. In general, solution trajectories cannot cross this *wall of singularities* except at the point $P(u, w) = Q(u, w) = 0$, called the *hole in the wall*, where the indeterminate form means that the system is no longer singular.

Since the discovery of these walls of singularities, they have been studied in a variety of biological (and other) applications [1, 18–20, 22–25, 29]. These studies (beginning with [24]) have led to the discovery of the possibility of both smooth and shock-fronted travelling wave solutions, arising as a result of the singular behaviour in the phase plane. Of particular interest is the transition from smooth to shock-fronted travelling waves and the role diffusive versus advective migration plays in determining the type of wavefront [20].

1.3. Geometric singular perturbation theory and canards. In [39], the authors studied the existence of shock-fronted travelling waves using methods from geometric singular perturbation theory (GSPT) with a particular focus on a special class of solutions known as *canards*.

The geometric approach to singular perturbation problems was introduced by [7]. As with other singular perturbation methods, geometric singular perturbation theory is applied to systems exhibiting two (or more) distinct time or length scales, indicated mathematically by a perturbation parameter multiplying the highest derivative. For a review of geometric singular perturbation methods see [11, 13], or as they apply to problems in mathematical biology [9]. These methods have been used to construct smooth travelling wave solutions to a bioremediation model [2], as well as to find pulse solutions to a three-component reaction-diffusion equation arising from a model for gas discharge dynamics [6]. However, these theorems only apply under the assumption of normal hyperbolicity, and break down in the neighbourhood

of points where normal hyperbolicity is lost, such as a wall of singularities. This is where the theory of canards comes into play.

The theory of canard solutions allows the extension of Fenichel theory to points in the neighbourhood of non-hyperbolic points [3, 17, 33, 36–38]. In [39], it was revealed that the *holes in the wall* investigated in [30, 31] using traditional phase plane analysis, are equivalent to the *folded singularities* investigated independently in [33, 34, 36] as part of the development of the existence of canards. We will use the latter approach.

1.4. The model. In this work, we study a model originally presented in [29]. The model describes haptotactic cell invasion in the context of malignant tumour growth, in particular melanoma (a type of skin cancer). In [29], the following simplified, dimensionless model is derived:

$$\frac{\partial c}{\partial t} = -c^2 u,$$
$$\frac{\partial u}{\partial t} = u(1 - u) - \frac{\partial}{\partial x}\left(\frac{\partial c}{\partial x} u\right),$$

with boundary conditions,

$$\lim_{x \to -\infty} c(x, t) = 0, \quad \lim_{x \to \infty} c(x, t) = \hat{c}, \quad \lim_{x \to -\infty} u(x, t) = 1, \quad \lim_{x \to \infty} u(x, t) = 0,$$

and $x \in \mathbb{R}$, $t \in \mathbb{R}^+$. Here $c(x, t)$ is the extracellular matrix (ECM) concentration and $u(x, t)$ is the invasive tumour cell population. Note that the original description of the tumour invasion process included an expression for the density of protease, but it was neglected as the density of protease can be assumed to be constant to leading order, within certain parameter regimes [25, 29]. The tumour cells proliferate logistically, independent of the presence of ECM, all the while consuming it. They also respond haptotactically to a gradient in ECM, and so migrate preferentially up the ECM gradient.

Haptotaxis is a type of advection similar to chemotaxis. Both describe the directed motion of cells up (down) the gradient of some chemical or chemoattractant (chemorepellent). Chemotaxis, as the better known term, arises when the chemoattractant (or chemorepellent) is suspended in a fluid. On the exterior of each cell are receptors that detect chemoattractant and allow it to pass into the cell. Based on the locations around the cell of the receptors admitting chemoattractant, the cells determine the most favourable migration direction. For example, if more receptors of the right hand side of the cell detect chemoattractant than on the left, the cell will move to the right. Thus, if a gradient in the chemoattractant is present, the cells will, on average, migrate up the chemical gradient. The opposite occurs in the case of a chemorepellent. Haptotaxis follows a similar mechanism but arises when the chemoattractant is bound to a surface. In this case, the concentration of cell adhesion sites could even act as a chemoattractant, as well as actual substrate-bound chemicals, such as present in the ECM.

Since the ECM is a substrate, to which the cells essentially bind themselves, it is reasonable to assume that diffusion plays a very small role in the tumour invasion process and therefore is ignored in [29]. (We shall not ignore diffusion but rather allow it to be small, see §1.5.)

In [29] and subsequently [24], the authors show that this model exhibits both smooth and shock-fronted travelling waves; we shall first provide a summary of the relevant results here, for more details we refer to the original works. Although the model was originally presented in [29], we focus on the analysis undertaken in the revised and self-contained version [24]. However, before we begin, we must address the issue of nomenclature. Within the travelling wave literature, it is convention to use c as the wavespeed of a travelling wave solution, not as a variable as in [24, 29]. Moreover, the model studied here fits the general framework of [39], and thus we choose to use the notation therein. Consequently, we let $c(x,t) = \tilde{u}(x,t)$, $u(x,t) = \tilde{w}(x,t)$ and will henceforth consider the system

$$
\begin{aligned}
\frac{\partial \tilde{u}}{\partial t} &= -\tilde{u}^2 \tilde{w}, \\
\frac{\partial \tilde{w}}{\partial t} &= \tilde{w}(1 - \tilde{w}) - \frac{\partial}{\partial x}\left(\frac{\partial \tilde{u}}{\partial x}\tilde{w}\right).
\end{aligned}
\tag{1.2}
$$

In order to investigate travelling wave solutions from a dynamical systems perspective, the coordinate transformation $z = x - ct$ is applied, where c is now the speed of the travelling wave. Thus (1.2) can be rearranged to the system of first order ODEs:

$$
\begin{aligned}
\frac{\mathrm{d}u}{\mathrm{d}z} &= \frac{u^2 w}{c}, \\
\left(\frac{2u^2 w}{c} - c\right)\frac{\mathrm{d}w}{\mathrm{d}z} &= w(1 - w) - \frac{2u^3 w^3}{c^2},
\end{aligned}
\tag{1.3}
$$

where we have dropped the tildes for convenience. The fixed points are $(1,0)$ and the line $(u_\infty, 0)$, where

$$
u_\infty(c) := \lim_{z \to \infty} u(z), \quad u_\infty \in \mathbb{R}.
$$

Identifying possible travelling waves of the PDE system (1.2) is equivalent to identifying heteroclinic orbits of the ODE system (1.3) connecting $(1,0)$ to $(u_\infty(c), 0)$.

Since (1.3) is now in the form (1.1), it exhibits a *wall of singularities* and a *hole in the wall* when analysing the phase plane. The wall of singularities is defined by the zeros of the term premultiplying the w-derivative,

$$
w = \frac{c^2}{2u^2} =: F(u).
\tag{1.4}
$$

The hole in the wall is defined as the point in the first quadrant, on the wall of singularities, where the right hand side of the w-equation also vanishes, and thus appears at the intersection of the wall of singularities (1.4) and the non-trivial w-nullcline. This gives

$$
(u_H, w_H) = \left(\frac{c}{4}\left[c + \sqrt{c^2 + 8}\right], \frac{1}{u_H + 1}\right).
\tag{1.5}
$$

By examining the phase plane, a two parameter family of heteroclinic orbits connecting $(0,1)$ to $(u_\infty, 0)$, representing both smooth (Type 1) and shock-fronted (Type 2) travelling waves were identified [24]. These orbits are constructed numerically, or using a power series

solution centered at (u_H, w_H) to approximate the two trajectories that cross through the wall of singularities, with the shocks defined by the Rankine–Hugoniot and Lax entropy conditions, see for example [32] and references within. Note that the power series solutions appear to provide a good approximation sufficiently far away from the $(0, 1)$ steady state.

The two parameters are the wavespeed c and the end state of the u-wave u_∞, which is equivalent to the parameter $\hat{c}$ in the original notation [24, 29]. The transition from the smooth to the shock-fronted waves is characterised by $u_\infty = u_{\text{crit}} = u_{\text{crit}}(c)$ or, equivalently, $c = c_{\text{crit}} = c_{\text{crit}}(u_\infty)$. Maximum and minimum values for u_∞ and c, respectively, are identified for the appearance of physically realistic (non-negative) shock-fronted waves.

An illustration of the different types of waves is given in Figure 1.1, emphasising the difference between the smooth and non-smooth waves. The solution curves for u are represented by the dashed lines and those for w by the solid lines. Initial conditions are shown in black, with the successive solutions plotted at equal time intervals. The different wave types were generated by varying the steepness of the initial profiles. This is discussed further in §3.1 and §3.2.
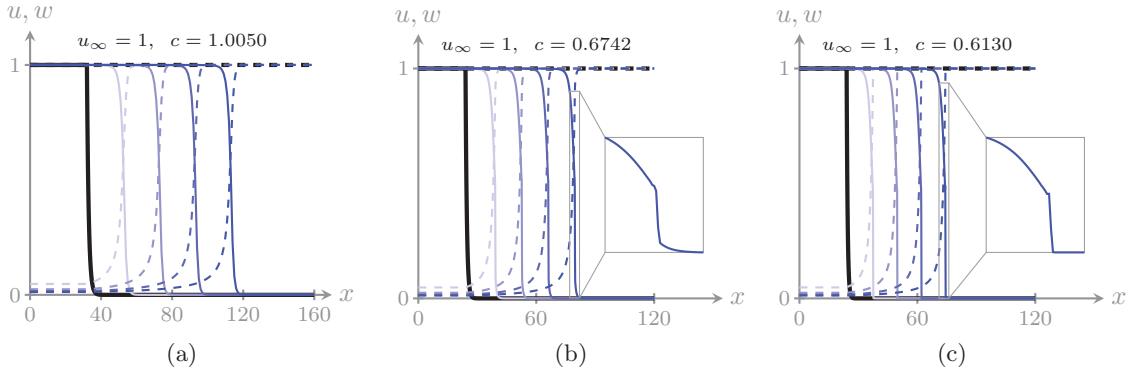

Figure 1.1: An illustration of the appearance of both smooth solutions and those exhibiting shock-like behaviour. The solutions are examples of a Type 1 wave, Type 2 wave with infinite support, and Type 2 wave with semi-compact support, from left to right. The solutions are generated from the numerical solution of (1.6) with $\varepsilon = 0.005$, however, are qualitatively the same as those presented in [24] for $\varepsilon = 0$. Dashed lines represent the u-solutions and solid lines the w-solutions, with initial conditions shown in black. Solutions are plotted at $t = 0, 20, \ldots, 80$.

In summary, it is concluded in [24] based on numerical evidence that *Type 1* solutions exist for $c \geq c_{\text{crit}}$ and *Type 2* solutions for $c_{\text{min}} < c \leq c_{\text{crit}}$, for fixed u_∞. Both wave types were demonstrated to be numerically stable. A third, *Type 3* wave was also considered, however, it did not satisfy the Lax entropy condition and was demonstrated to be numerically unstable. Waves for which $c < c_{\text{min}}$ were not considered as they would be non-physical. These results can also be expressed in terms of ranges of the parameter u_∞, for fixed c.

The existence of the Type 1 waves is rigorously proven in [10] by considering a desingularised version of (1.3) and constructing an invariant region to which the Type 1 waves are

restricted.

1.5. Outline and main results. In this work we formalise the results from [24], and extend the work of [10], to provide a rigorous proof of existence of both smooth and shock-fronted travelling wave solutions to (1.2). Furthermore, we prove the existence of travelling wave solutions for the more general model, where both the ECM and cell species are allowed to diffuse,

$$
\begin{aligned}
u_t &= -u^2 w + \varepsilon u_{xx}, \\
w_t &= w(1-w) - (u_x w)_x + \varepsilon w_{xx},
\end{aligned}
\tag{1.6}
$$

with $x \in \mathbb{R}$, $t \in \mathbb{R}^+$ and $\varepsilon \ll 1$. From a biological or modelling perspective, this formulation is advantageous as it allows us to investigate the effects of small diffusion, as well as no diffusion. (Note that for $\varepsilon = 0$, (1.6) is equivalent to (1.2).) We take the diffusion coefficients to be equal for simplicity. However, if we instead chose diffusion coefficients such that the ratio was $\mathcal{O}(1)$ but not equal to 1, the method used would carry through and the results would not be significantly altered, as stated in [39, Remark 2.1].

The background states of (1.6) are $(u, w) = (0, 1)$ and $(u, w) = (u_\infty, 0)$, $u_\infty \in \mathbb{R}$; that is, $(u_\infty, 0)$ represents a line of fixed points. Hence, we are searching for travelling wave solutions on an unbounded domain that connect $(0, 1)$ (representing a state with no ECM and a dimensionless concentration of 1 of tumour cells) to $(u_\infty, 0)$ (representing the tumour free state with a variable amount of ECM). Thus, we have

$$
\lim_{z \to -\infty} u(z) = 0, \quad \lim_{z \to \infty} u(z) = u_\infty, \quad \lim_{z \to -\infty} w(z) = 1, \quad \lim_{z \to \infty} w(z) = 0.
\tag{1.7}
$$

Due to the nature of the background states and the expectation that the tumour cells will invade the ECM, we expect to see right-moving travelling waves, that is $c > 0$. The second condition in (1.7) implies that the right hand boundary condition on u, denoted u_∞, is free. Since u and w represent concentrations, we shall focus on solutions to (1.6) for which $u, w \in [0, \infty)$ for all $x \in \mathbb{R}$, $t \in \mathbb{R}^+$. Hence, for this purpose we assume $u_\infty \geq 0$. We will however, consider one type of solution for which $w < 0$.

From a mathematical perspective, the advantage of the formulation (1.6) over (1.2) lies in the applicability of GSPT to (1.6), as demonstrated in [39]. In [39], travelling wave solutions of the general model (to which (1.6) conforms),

$$
\begin{pmatrix} u \\ w \end{pmatrix}_t + \begin{pmatrix} 0 \\ g(u,w)u_x \end{pmatrix}_x = \begin{pmatrix} h(u,w) \\ f(u,w) \end{pmatrix} + \varepsilon \begin{pmatrix} u \\ w \end{pmatrix}_{xx},
\tag{1.8}
$$

are investigated, with $f(u,w)$, $g(u,w)$ and $h(u,w)$ adhering to certain assumptions. We explicitly check these assumptions for (1.6). Upon introducing a new variable $v = u_x$, (1.8) is transformed into the singularly perturbed system of coupled balance laws:

$$
\begin{pmatrix} u \\ v \\ w \end{pmatrix}_t + \begin{pmatrix} 0 \\ -h(u,w) \\ g(u,w)v \end{pmatrix}_x = \begin{pmatrix} h(u,w) \\ 0 \\ f(u,w) \end{pmatrix} + \varepsilon \begin{pmatrix} u \\ v \\ w \end{pmatrix}_{xx},
\tag{1.9}
$$

where we note that the first two equations are equivalent since the second is the derivative (with respect to x) of the first. Consequently, GSPT, including Fenichel theory [7] and the

theory of canard solutions [17, 33, 36–38], is used to provide a general framework for a proof of the existence of travelling wave solutions of (1.8). These solutions include smooth travelling waves, as well as those that exhibit shock-like behaviour.

The key steps of the proof are as follows:
- reformulate the model as a singular perturbation problem as in (1.9);
- in the singular limit $\varepsilon \to 0$, identify *fold(s)* in the *critical manifold* (see Lemma 2.2);
- identify *folded saddle canard point(s)* (see Lemma 2.4);
- construct heteroclinic orbits (see Lemmas 2.5, 2.6 and 2.7);
- prove the persistence of the singular heteroclinic orbits for sufficiently small $\varepsilon > 0$ (see §2.5).

Note that the folded nature of the critical manifold is essential for the existence of shock-fronted travelling wave solutions in the limit $\varepsilon \to 0$. Furthermore, the existence of the folded saddle canard point is an important feature of such models as (1.8) that was previously unrecognised.

In §2, following the steps outlined above we identify singular heteroclinic orbits representing so called Type I, II, III and IV waves. The classification of the travelling wave solutions as Type I, II, III or IV is based on distinguishing features of the waves in the singular limit $\varepsilon \to 0$. Figure 1.2 provides an illustration of the four types of waves. We assume the label for the Type 1 waves from [24], that is, any smooth travelling waves are classified as Type I. The Type 2 waves identified by [24] are waves that exhibit a shock in w, including both those with infinite and semi-compact support. We split this category in two; Type II waves, which are the Type 2 waves from [24] with infinite support, and Type III waves, which have semi-compact support in w. The reason for the explicit distinction between the Type II and III waves will become apparent in §3. Note that the Type III waves should not be confused with the Type 3 waves from [24], which we show do not exist. The Type IV waves are those that exhibit a shock and have a negative component in w. This type of solution was not considered in [24] as it is non-physical.

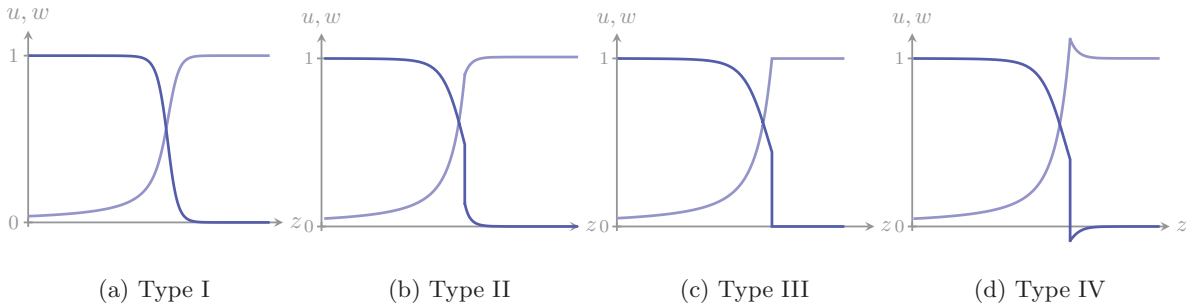(a) Type I   (b) Type II   (c) Type III   (d) Type IV

Figure 1.2: Illustration of the four types of travelling wave solutions identified.

Having completed the proof of existence, in §3 we present additional numerical results, in particular, relating to the wavespeeds of the various travelling wave solutions. We derive an expression for the wavespeed of Type I and II waves that compares well with the numerically measured wavespeeds. However, an expression for the wavespeed of the Type III, minimum

wavespeed wave remains to be found. No Type IV waves were observed numerically. We conclude in §4.

2. Existence. In this section we prove the existence and uniqueness of travelling wave solutions to (1.6) for sufficiently small ε, by means of dynamical systems theory and in particular, GSPT. These solutions include both travelling waves with and without a *shock*.

Before we begin we wish to make clear what we mean by a *shock* or a *shock-fronted* travelling wave, based on classical PDE theory. For $\varepsilon = 0$, the system is strictly hyperbolic and so is known to exhibit shocks. These shocks are defined by the Rankine–Hugoniot and Lax conditions. Thus for $\varepsilon = 0$, when we talk about solutions exhibiting a *shock* we are referring to weak solutions of (1.2), which contain discontinuities, with the solution away from the discontinuity satisfying (1.2) and the discontinuity satisfying the appropriate shock conditions. As we turn on ε these discontinuities smooth out and thus the entire solution will satisfy (1.6). However, for $0 < \varepsilon \ll 1$ sufficiently small the solutions will still contain regions with steep gradients where the discontinuity was previously observed.

Thus, when we refer to a *shock* we are referring to the region in a solution containing very steep gradients, which in the limit $\varepsilon \to 0$ becomes a discontinuity. From a geometric perspective, the *shocks* correspond to components of the solutions that arise from a diversion through the fast subsystem. Futhermore, the corresponding Rankine–Hugoniot and Lax entropy conditions for hyperbolic PDEs have a clear geometric interpretation.

Theorem 2.1. *There exists an ε_0 such that for $\varepsilon \in [0, \varepsilon_0]$ travelling wave solutions exist for the system (1.6) with boundary conditions (1.7), and are unique in the sense that for a given $c > 0$ and $u_\infty > 0$, a single wave exists. Furthermore, for fixed wavespeeds and $u_\infty > 0$ four wave types can be identified. The Type I wave exists for $0 < u_\infty < u_{\mathrm{crit}}$, and is smooth. The Type II wave exists for $u_{\mathrm{crit}} < u_\infty < u_3$, and exhibits a shock in w. The Type III wave exists for $u_\infty = u_3$, and exhibits a shock and has semi-compact support in w. The Type IV wave exists for $u_3 < u_\infty < u_{\mathrm{upper}}$, and exhibits a shock and has a negative component in w.*

We follow [39] and begin by introducing a new variable, $v = u_x$, such that we can write (1.6) as a system of coupled balance laws,

$$
\begin{aligned}
u_t &= -u^2 w + \varepsilon u_{xx}, \\
v_t &= -(u^2 w)_x + \varepsilon v_{xx}, \\
w_t &= w(1-w) - (vw)_x + \varepsilon w_{xx}.
\end{aligned}
\tag{2.1}
$$

Since we are looking for travelling wave solutions we introduce the coordinate $z = x - ct$, where $c > 0$. This gives

$$
\begin{aligned}
(\varepsilon u' + cu)' &= u^2 w, \\
(\varepsilon v' - u^2 w + cv)' &= 0, \\
(\varepsilon w' - vw + cw)' &= -w(1-w),
\end{aligned}
\tag{2.2}
$$

where the prime indicates differentiation with respect to z. Defining three new variables

$$
\begin{aligned}
\hat{u} &:= \varepsilon u' + cu, \\
\hat{v} &:= \varepsilon v' - u^2 w + cv, \\
\hat{w} &:= \varepsilon w' - vw + cw,
\end{aligned}
$$

allows us to write (2.2) as a system of first order differential equations,

$$\begin{aligned}
\hat{u}' &= u^2 w, \\
\hat{v}' &= 0, \\
\hat{w}' &= -w(1-w), \\
\varepsilon u' &= \hat{u} - cu, \\
\varepsilon v' &= \hat{v} + u^2 w - cv, \\
\varepsilon w' &= \hat{w} + vw - cw.
\end{aligned}$$

The second equation implies $\hat{v}$ is a constant. Moreover, it can be seen upon comparison of the definition of $\hat{v}$ and the first equation of (2.2) (recalling that $v = u'$), that $\hat{v} = 0$. Therefore, we now have a five-dimensional, singular perturbation problem:

$$\begin{aligned}
\hat{u}' &= u^2 w, \\
\hat{w}' &= -w(1-w), \\
\varepsilon u' &= \hat{u} - cu, \\
\varepsilon v' &= u^2 w - cv, \\
\varepsilon w' &= \hat{w} + vw - cw,
\end{aligned} \tag{2.3}$$

containing two slow variables ($\hat{u}$ and $\hat{w}$) and our three, original fast variables (u, v and w). We refer to (2.3) as the five-dimensional *slow system*, with z the *slow travelling wave coordinate*. To investigate the problem on the fast timescale we introduce the *fast travelling wave coordinate* $y = z/\varepsilon$, which gives the corresponding five-dimensional *fast system*:

$$\begin{aligned}
\dot{\hat{u}} &= \varepsilon u^2 w, \\
\dot{\hat{w}} &= -\varepsilon w(1-w), \\
\dot{u} &= \hat{u} - cu, \\
\dot{v} &= u^2 w - cv, \\
\dot{w} &= \hat{w} + vw - cw,
\end{aligned} \tag{2.4}$$

provided $\varepsilon \neq 0$ and where the dot indicates differentiation with respect to y.

The non-trivial fixed points of the five-dimensional systems, denoted $P_{\mp}$ for the respective end states of the wave, are $P_-(\hat{u}, \hat{w}, u, v, w) = (0, c, 0, 0, 1)$ and $P_+(\hat{u}, \hat{w}, u, v, w) = (cu_\infty, 0, u_\infty, 0, 0)$.

As per geometric singular perturbation theory, we now examine the singular limit of the slow and fast systems, (2.3) and (2.4), respectively. This provides us with two lower-dimensional problems, which are consequently more amenable to analysis. In the singular limit $\varepsilon \to 0$ the five-dimensional slow system (2.3) reduces to the two-dimensional *reduced*

problem with three algebraic constraints:

$$\begin{aligned}
\hat{u}' &= u^2 w, \\
\hat{w}' &= -w(1-w), \\
0 &= \hat{u} - cu, \\
0 &= u^2 w - cv, \\
0 &= \hat{w} + vw - cw.
\end{aligned} \tag{2.5}$$

Similarly, as $\varepsilon \to 0$ the five-dimensional fast system (2.4) reduces to the three-dimensional *layer problem* with two parameters:

$$\begin{aligned}
\dot{\hat{u}} &= 0, \\
\dot{\hat{w}} &= 0, \\
\dot{u} &= \hat{u} - cu, \\
\dot{v} &= u^2 w - cv, \\
\dot{w} &= \hat{w} + vw - cw.
\end{aligned} \tag{2.6}$$

Given the above two subsystems, GSPT allows us to study each independently, and construct singular limit solutions that are concatenations of solution segments of both subsystems. Then, assuming certain conditions are met, we can prove that the singular limit solutions perturb to nearby solutions of the full, five-dimensional problem for $0 < \varepsilon \ll 1$.

2.1. Layer problem. We begin our analysis with the layer problem (2.6) and note that within the layer problem the slow variables are constants of integration and so the layer flow is independent of the slow variables, or is along so called *fast fibres*. A diversion of the solution through the fast subsystem, or equivalently along a fast fibre, corresponds to a shock in the travelling wave solution. Thus, this condition implies that the slow variables will be constant along any shocks in the travelling wave solutions.

The steady states of the layer problem (2.6) define a two-dimensional critical surface or critical manifold, which can be represented as a graph over the fast variables (u, w):

$$S = \left\{ (\hat{u}, \hat{w}, u, v, w) \ \middle| \ \hat{u} = cu, v = \frac{u^2 w}{c}, \hat{w} = cw - vw \right\}. \tag{2.7}$$

While this is not the only possible graph representation of the set S, we emphasise that it is not possible to describe S as a graph over a slow variable base. This follows from the following:

Lemma 2.2. *The layer problem* (2.6) *has a saddle-node bifurcation along the set $F(u)$ defined in* (1.4). *That is, the critical manifold S, defined in* (2.7), *is folded around $F(u)$, with one attracting side, S_a, and one repelling, S_r. Moreover, S is symmetric in w around $F(u)$.*

Proof. The Jacobian of the layer problem,

$$J = \begin{bmatrix} -c & 0 & 0 \\ 2uw & -c & u^2 \\ 0 & w & -c+v \end{bmatrix},$$

evaluated along S, has eigenvalues given by

$$\lambda_1 = -c,$$

$$\lambda_{2,3} = -c + \frac{u^2 w}{2c} \pm \sqrt{\left(\frac{u^2 w}{2c}\right)^2 + u^2 w}.$$

The eigenvalues λ_1 and λ_3 are negative for $u, w \geq 0$, whereas λ_2 can change sign. Thus, for $\lambda_2 < 0$ $(2u^2 w < c^2)$ S is stable or attracting (denoted S_a) and for $\lambda_2 > 0$ $(2u^2 w > c^2)$ is unstable or repelling (denoted S_r).

The loss of normal hyperbolicity at $\lambda_2 = 0$ is generically due to either a Hopf or saddle-node (fold) bifurcation. In this case, since λ_2 also has zero imaginary part, we have a saddle-node bifurcation. This implies that the critical manifold is folded, provided the non-degeneracy and transversality conditions,

$$\boldsymbol{p} \cdot (D^2_{\boldsymbol{UU}} \boldsymbol{G})(\boldsymbol{U}, \hat{\boldsymbol{U}})(\boldsymbol{q}, \boldsymbol{q}) \neq 0 \quad \text{and} \quad \boldsymbol{p} \cdot (D_{\hat{\boldsymbol{U}}} \boldsymbol{G})(\boldsymbol{U}, \hat{\boldsymbol{U}}) \neq \boldsymbol{0}$$

respectively, are met [38]. Here $\boldsymbol{U} = (u, v, w)$, $\hat{\boldsymbol{U}} = (\hat{u}, \hat{w})$ and $\boldsymbol{G} = (\dot{u}, \dot{v}, \dot{w})$, with $\dot{u}$, $\dot{v}$ and $\dot{w}$ defined in (2.6), and where $\boldsymbol{U}$ and $\hat{\boldsymbol{U}}$ are evaluated along $\lambda_2 = 0$, which coincides with $w = F(u)$ as in (1.4). Therefore, $\boldsymbol{U} = (u, v, w) = (u, c/2, c^2/(2u^2))$. The vectors $\boldsymbol{p}$ are $\boldsymbol{q}$ and the left and right null vectors of J respectively, with $\boldsymbol{q} \cdot \boldsymbol{q} = \boldsymbol{p} \cdot \boldsymbol{q} = 1$:

$$\boldsymbol{p} = \frac{1}{P}\left(\frac{c^4}{2u^3}, \frac{c^3}{2u^2}, c^2\right), \quad \boldsymbol{q} = \frac{1}{Q}\left(0, u^2, c\right)^T,$$

where

$$P = \frac{3c^3}{2Q}, \quad Q = \sqrt{c^2 + u^4}.$$

The first condition is equivalent to showing that $\boldsymbol{p} \cdot \boldsymbol{B}(\boldsymbol{q}, \boldsymbol{q}) \neq 0$, where

$$\boldsymbol{B}_i(\boldsymbol{q}, \boldsymbol{q}) = \sum_{j,k} \frac{\partial^2 \boldsymbol{G}_i}{\partial \boldsymbol{U}_k \partial \boldsymbol{U}_j} \boldsymbol{q}_j \boldsymbol{q}_k$$

with the derivatives, as well as $\boldsymbol{U}_j$ and $\boldsymbol{U}_k$ evaluated along $\lambda_2 = 0$. This gives

$$\boldsymbol{B}(\boldsymbol{q}, \boldsymbol{q}) = \left(0, 0, \frac{2cu^2}{Q^2}\right)^T,$$

and

$$\boldsymbol{p} \cdot \boldsymbol{B}(\boldsymbol{q}, \boldsymbol{q}) = \frac{2c^3 u^2}{PQ^2},$$

which is non-zero for $c \neq 0$ and $u \neq 0$.

The second condition reduces to

$$\boldsymbol{p} \cdot \begin{bmatrix} 1 & 0 \\ 0 & 0 \\ 0 & 1 \end{bmatrix} = \left(\frac{c^4}{2u^3 P}, \frac{c^2}{P}\right) \neq \boldsymbol{0}.$$

Therefore, the critical manifold S is folded with the fold curve corresponding to where $\lambda_2 = 0$ or $2u^2w = c^2$. This fold curve is equivalent to the wall of singularities (1.4) found in [24].

Furthermore, on S we have

$$\hat{w}(u, v(u, w), w)|_{w=F(u)+A} = \hat{w}(u, v(u, w), w)|_{w=F(u)-A},$$

where A is an arbitrary constant. Consequently, S is symmetric in w around the fold line and points on S connected by fast fibres will be equidistant from the fold line in the w-variable. Defining $w_\pm \in S_{r,a}$ to be the values of w at either end of the fast fibre we have

$$w = F(u) = \frac{w_+ + w_-}{2}. \tag{2.8}$$

To visualise the two-dimensional manifold S defined in the five-dimensional (phase-)space, we plot projections in three-dimensional subspaces:

$$\hat{w} = cw - \frac{u^2w^2}{c} \qquad \text{or} \qquad \hat{w} = \frac{c^2v - cv^2}{u^2}, \tag{2.9}$$

as seen in the left and right hand panels of Figure 2.1, respectively, with the black line indicating the fold curve, F. Note that a consequence of the folded nature of S is that it can not be expressed in a single coordinate chart over the slow variables $(\hat{u}, \hat{w})$, as seen in Figure 2.1 (where since $c = 1$, $\hat{u} = u$ on S). The fast fibres mentioned previously connect points on S with constant $\hat{u}$ and $\hat{w}$. Due to the stability of S, the direction of the flow along these fast fibres is from the S_r to S_a, see Figure 2.2.
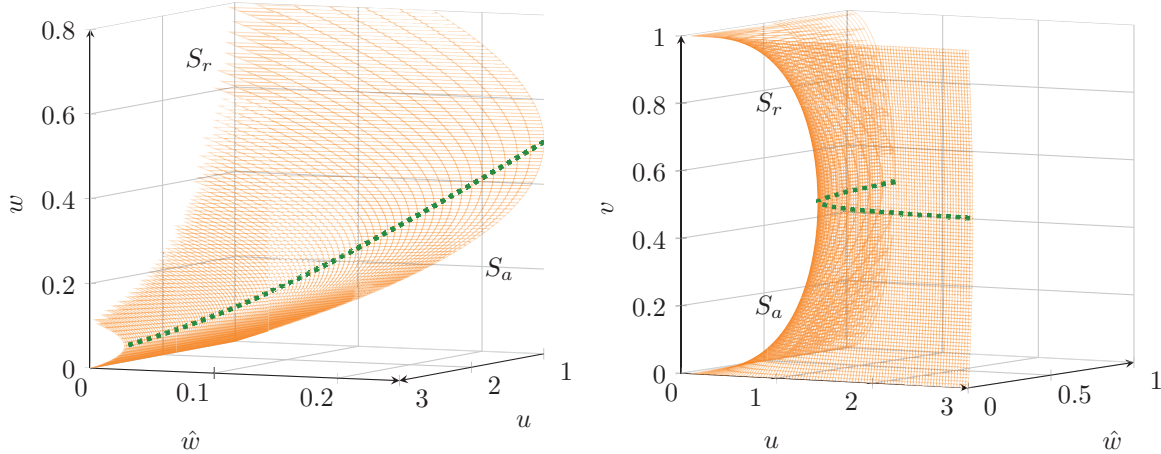

Figure 2.1: Projections of the critical manifold S (2.7) defined in (2.9) for $c = 1$. The green, dotted line represents the fold curve. The left hand figure plots S projected onto $(u, \hat{w}, w)$-space. The right hand figure plots S projected onto $(u, \hat{w}, v)$-space, so as to more easily observe the folded nature of the critical manifold.
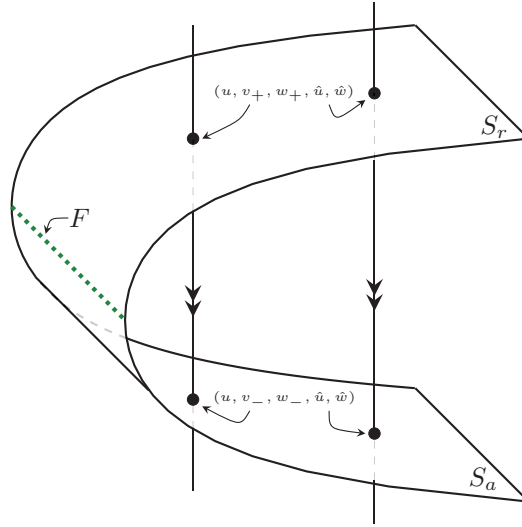
Figure 2.2: A schematic of the critical manifold S. The fold curve F is represented by the dashed, green line. The upper part of the surface is the repelling side of the manifold S_r and the lower part the attracting side of the manifold S_a. The flow of the layer problem is along *fast fibres*, two examples of which are drawn in. They connect a point on S_r (labelled $(u, v_+, w_+, \hat{u}, \hat{w})$), to a point of S_a (labelled $(u, v_-, w_-, \hat{u}, \hat{w})$). Along these fast fibres u, $\hat{u}$ and $\hat{w}$ are constant. The direction of the flow can only be in that shown here; that is, from S_r to S_a.

Remark 2.3. For $\varepsilon = 0$ and $u, w > 0$, (2.1) is strictly hyperbolic, and so solutions can exhibit shocks. These shocks must satisfy the Rankine–Hugoniot and Lax entropy conditions, which are given in [24]. The Rankine–Hugoniot conditions can be written:

$$cu_+ = cu_-,$$

$$v_+ - v_- = \frac{u^2}{c}(w_+ - w_-),$$

$$cw_+ - v_+ w_+ = cw_- - v_- w_-,$$

where the $\pm$ subscript denotes the value of the given variable at the beginning or end state of the shock respectively. By comparing these conditions with the definition of S in (2.7), we see that they are satisfied since $\hat{u}$ and $\hat{w}$ are constant along any shocks in the system. Furthermore, the second and third conditions combined, can be rearranged to give (2.8). The Lax entropy condition reduces simply to $w_+ > w_-$, but can also be written as

$$2u^2 w_- < c^2 < 2u^2 w_+.$$

This implies that the direction of the shock must be from the repelling to the attracting side of the manifold.

Hence, the combinations of slow variables being constant within the layer problem, and the shape and stability of the critical manifold encapsulate the restrictions imposed by the

Rankine–Hugoniot and Lax entropy conditions and discussed in [24]. Note that the Lax entropy condition is not satisfied for the Type 3 waves in [24], and consequently they do not exist.

2.2. Reduced problem. The reduced problem (2.5) is a differential-algebraic problem, that is, the reduced flow is constrained to a manifold. This implies that the reduced vector field must be in the tangent bundle of the critical manifold S. Since S is given as a graph over (u, w)-space we can study the reduced flow in the single coordinate chart (u, w).

Lemma 2.4. *The reduced problem contains a folded saddle canard point.*

Proof. We substitute the definitions of $\hat{u}$ and $\hat{w}$ in (2.7) into the differential equations of (2.5), to obtain the reduced vector field on S, written in matrix form:

$$
\begin{bmatrix} \hat{u} \\ \hat{w} \end{bmatrix}' = M \begin{bmatrix} u \\ w \end{bmatrix}' := \begin{bmatrix} c & 0 \\ -2uw^2/c & c - 2u^2w/c \end{bmatrix} \begin{bmatrix} u \\ w \end{bmatrix}' = \begin{bmatrix} u^2w \\ -w(1-w) \end{bmatrix},
$$

where the prime indicates differentiation with respect to the *slow* variable z and M is singular along $2u^2w = c^2$, the fold curve or wall of singularities. We multiply both sides by the cofactor matrix of M,

$$
\begin{bmatrix} c - 2u^2w/c & 0 \\ 2uw^2/c & c \end{bmatrix},
$$

to give

$$
\{c^2 - 2u^2w\} \begin{bmatrix} u \\ w \end{bmatrix}' = \begin{bmatrix} cu^2w - 2u^4w^2/c \\ -cw(1-w) + 2u^3w^3/c \end{bmatrix}. \tag{2.10}
$$

The above system is still singular for $2u^2w = c^2$, but the singularity can be removed by rescaling the independent variable $\bar{z}$, such that

$$
\frac{\mathrm{d}z}{\mathrm{d}\bar{z}} = c^2 - 2u^2w. \tag{2.11}
$$

This gives the desingularised system,

$$
\begin{aligned}
\frac{\mathrm{d}u}{\mathrm{d}\bar{z}} &= cu^2w - \frac{2u^4w^2}{c}, \\
\frac{\mathrm{d}w}{\mathrm{d}\bar{z}} &= -cw(1-w) + \frac{2u^3w^3}{c}.
\end{aligned} \tag{2.12}
$$

The equilibrium points of (2.12) are $(u_U, w_U) = (0, 1)$, $(u_S, w_S) = (u_\infty, 0)$, $u_\infty \in \mathbb{R}$ and

$$
(u_H, w_H) = \left(\frac{c}{4} \left[c + \sqrt{c^2 + 8} \right], \frac{1}{u_H + 1} \right). \tag{2.13}
$$

The former equilibrium points correspond to the background states of (1.6) given in (1.7), while the latter is a product of the desingularisation. More specifically: $(u_U, w_U) = (0, 1)$ has eigenvalues and eigenvectors

$$
\lambda_1 = c, \quad \boldsymbol{\psi}_1 = (0, 1), \quad \lambda_2 = 0, \quad \boldsymbol{\psi}_2 = (1, 0),
$$

and is therefore centre-unstable; $(u_S, w_S) = (u_\infty, 0)$ has eigenvalues and eigenvectors

$$\lambda_1 = -c, \quad \psi_1 = (-u_\infty^2, 1), \quad \lambda_2 = 0, \quad \psi_2 = (1, 0),$$

and is therefore centre-stable; and finally, (u_H, w_H) has eigenvalues and eigenvectors

$$\lambda_\pm = \left(\frac{c - \sqrt{c^2 + 8}}{2} \right)^4 \left[1 \pm c \sqrt{\left(\frac{4}{c - \sqrt{c^2 + 8}} \right)^4 - 3} \right], \quad \psi^\pm = (f^\pm(c), -1),$$

and is therefore a saddle (we consider $f^\pm(c)$ in more detail in §2.4). The phase portrait of (2.12) is shown in Figure 2.3a, with u and w parameterised by $\bar{z}$.

To obtain the (u, w)-phase portrait parameterised by z, we observe that $\dfrac{\mathrm{d}z}{\mathrm{d}\bar{z}} > 0$ on S_a (that is, below the fold curve F), while $\dfrac{\mathrm{d}z}{\mathrm{d}\bar{z}} < 0$ on S_r. Therefore, the direction of the trajectories in the $(u(z), w(z))$-phase portrait will be in the opposite direction to those in the $(u(\bar{z}), w(\bar{z}))$-phase portrait for trajectories on S_r, but in the same direction for trajectories on S_a. This does not affect the stability or type of the fixed points (u_U, w_U) and (u_S, w_S). However, (u_H, w_H) is not a fixed point of (2.10).

Rather, as the direction of the trajectories on S_r are reversed, the saddle equilibrium of (2.12) becomes a *folded saddle* canard point of (2.10) [39], equivalent to the hole in the wall (1.5). In particular, on S_r the stable (unstable) eigenvector of the saddle equilibrium of (2.12) becomes the unstable (stable) eigenvector of the folded saddle canard point. This allows two trajectories to pass through (u_H, w_H): one from S_a to S_r and one from S_r to S_a. We refer to the former as the *canard* solution and the latter the *faux canard* solution. In Figure 2.4, the canard solution is the union of $\mathcal{W}_*^S$ and T_{off}, and the faux canard solution on S_r is depicted as $\mathcal{W}_{\text{crit}}^U$. The (u, w)-phase portrait parameterized by z is shown in Figure 2.3b. ■

Since all the equilibrium points of (2.10) lie on S_a, there are only two possible ways to create heteroclinic orbits. Firstly, smooth connections can be made (on S_a) to the u_∞ steady states up to a critical value of u_∞, which we call u_{crit}. These heteroclinic orbits correspond to smooth travelling wave solutions and are the Type 1 waves identified in [24]. In this case, the connections are made purely on S_a, that is without crossing through the canard point onto S_r. The second possibility for creating heteroclinic connections arises if the solution does cross through the canard point onto S_r. This case is considered in §2.3.

Lemma 2.5. *For $0 < u_\infty \leq u_{\text{crit}}$, $u_{\text{crit}} \in (u_H, \infty]$, there exist singular heteroclinic orbits $\Gamma = \gamma_s$ representing Type I waves; that is, singular heteroclinic orbits that live solely on S_a.*

Proof. From the phase plane analysis we know that for $u < u_H$, $w < 1$, trajectories cross the w-nullcline N from left to right, and travel along the $\{u = 0\}$-nullcline in a downward direction. Furthermore, a calculation comparing the gradient of N with the stable eigenvector of the canard point (on S_a) reveals that the canard solution enters the canard point under N. Finally, it can be shown using a monotonicity argument for the derivative

$$\frac{\mathrm{d}w}{\mathrm{d}u} = -\frac{c^2(1 - w) - 2u^3 w^2}{u^2(c^2 - 2u^2 w)}, \tag{2.14}$$

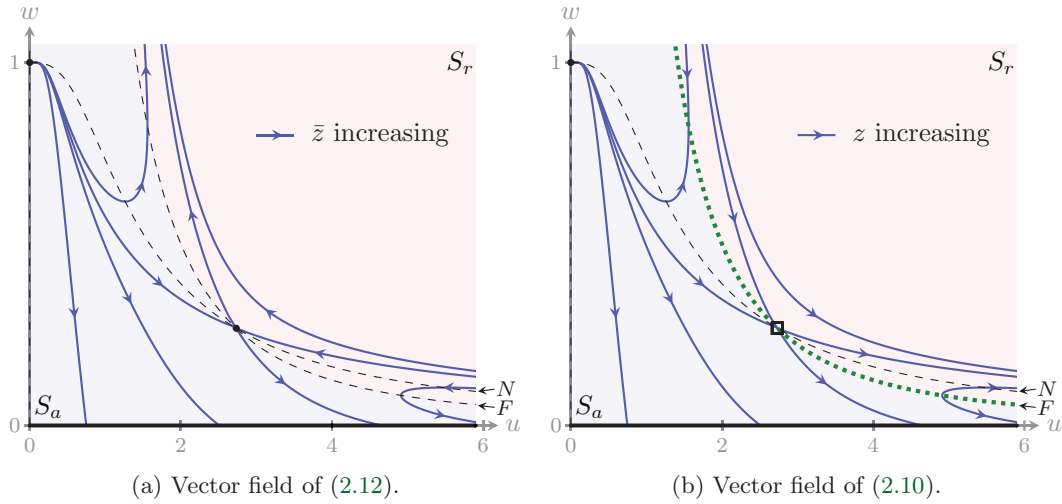(a) Vector field of (2.12).   (b) Vector field of (2.10).

Figure 2.3: The left and right hand figures show the (u, w)-phase portraits parameterised by $\bar{z}$ and z, respectively. The fold curve is labelled F and the non-trivial u-nullcline N with the saddle equilibrium (filled black circle), and folded saddle canard point (open black square) visible at the intersection of these curves, in the left and right hand figures respectively. The other black circles correspond to the background states of (1.6), which are fixed points of both (2.10) and (2.12), with the thick black line along the u-axis indicating that the whole axis is a steady state. Trajectories representing travelling wave solutions connect the unstable steady state $(0, 1)$ to any of the family of stable steady states $(u_\infty, 0)$ along the u-axis. The region below F, shaded blue corresponds to the attracting side of the critical manifold S_a, and above F, shaded red to the repelling side S_r.

that in Figure 2.3b all solutions on S_a (S_r) and below (above) N will be monotonically decreasing in w and consequently increasing in u [29]. (This is indicated in Figure 2.4 by the direction of the blue arrows.) Together, these conditions guarantee that the component of the canard solution on S_a connects (u_H, w_H) to the unstable steady state $(u, w) = (0, 1)$ (in backward z). We denote this trajectory $\mathcal{W}_*^S$; see Figure 2.4.

Similarly, due to monotonicity, the component of the faux canard solution on S_a connects (u_H, w_H) to a stable steady state $(u, w) = (u_{\text{crit}}, 0)$, $u_{\text{crit}} \in (u_H, \infty)$ in forward z. We denote this trajectory $\mathcal{W}_{\text{crit}}^U$, as in Figure 2.4.

The two trajectories $\mathcal{W}_*^S$ and $\mathcal{W}_{\text{crit}}^U$, along with the u- and w-axes act as separatrices that bound the region in which smooth heteroclinic connections can be made on S_a. Therefore, any trajectory leaving $(0, 1)$ with a gradient less than $\mathcal{W}_*^S$, will make a smooth connection on S_a to $(u_\infty, 0)$, $u_\infty \in (0, u_{\text{crit}})$. Since a singular heteroclinic orbit Γ representing a Type I wave consists of a single slow segment γ_s, we have simply $\Gamma = \gamma_s$. ∎

An example of a Type I wave, with the corresponding phase trajectory is shown in Figure 2.5a.

2.3. Travelling waves with shocks. The second way to connect the steady states is by concatenating solutions from the reduced and layer problems.

Lemma 2.6. *For $u_\infty > u_{\text{crit}}$, there exist singular heteroclinic orbits $\Gamma = \gamma_c \cup \gamma_f \cup \gamma_s$ representing Type II waves.*

Proof. Type II waves correspond to solutions that follow $\mathcal{W}_*^S$ and pass through the folded saddle canard point (u_H, w_H) onto S_r. Once on S_r the solution can then switch onto a fast fibre of the layer problem, which connects a point on S_r to the point on S_a with constant $\hat{u}$ and $\hat{w}$. We refer to this action as a *jump* or *shock*. Since $u = \hat{u}/c$ on S, the value of u at either end of the shock will also be constant. The values of w at either end (denoted $w_\pm$) are the solutions of (2.9) for the given values of $\hat{w}$ and u. Alternatively, if the value of w at one end of the shock is known, the value at the other end can be computed from (2.8).

Once the solution has returned to S_a via the fast fibre, monotonicity guarantees that the solution trajectory continues to a stable steady state $(u_\infty, 0)$, thus completing the heteroclinic orbit. For Type II waves, we are assuming that the jump lands at a point on S_a with $w > 0$.

Thus, a singular heteroclinic orbit Γ representing a Type II wave is a concatenation of three components: γ_c, the slow segment of the orbit that follows that canard solution; γ_f, the fast segment of the orbit along a fast fibre; and γ_s, the remaining slow component of the orbit that connects to the end state $(u_\infty, 0)$. ∎

We define the take-off curve $T_{\text{off}}(u)$ as the set of points $(u, w_+ = T_{\text{off}}(u))$ from which the solution leaves S_r and switches onto a fast fibre of the layer problem. Note that T_{off} coincides with the canard solution on S_r. Similarly, we define the touch-down curve $T_{\text{down}}(u)$ as the set of points $(u, w_- = T_{\text{down}}(u))$ on S_a to which the fast fibres connect, or equivalently, the landing points of any jumps in the solution. These curves are illustrated in Figure 2.4. Both T_{off} and T_{down} are monotonically decreasing functions of u and as a result $u \geq u_H$ and $w \leq w_H$ along T_{off} and T_{down}.

If T_{down} intersects the u-axis at say, $u = u_3$ (with $u_3 \in (u_H, \infty)$ as labelled in Figure 2.4), then there is the possibility for jumps to land on S_a with $w \leq 0$, as opposed to with $w > 0$ as is the case for a Type II wave. It is worth noting that in all the cases we tested numerically, $u_3 < \infty$.

Lemma 2.7. *If $u_3 < \infty$, that is, T_{down} intersects the u-axis, then there exist singular heteroclinic orbits Γ representing Type III ($\Gamma = \gamma_c \cup \gamma_f$) and Type IV ($\Gamma = \gamma_c \cup \gamma_f \cup \gamma_s$) waves.*

Proof. The Type III wave corresponds to the special case where the jump or fast fibre connects the solution trajectory directly to the stable steady state $(u_3, 0)$. Due to this direct connection, Type III waves have semi-compact support, in contrast to Type II waves, which have infinite support. Furthermore, the direct connection implies a singular heteroclinic orbit Γ representing a Type III wave is a concatenation of only two components, $\Gamma = \gamma_c \cup \gamma_f$. For the Type III wave, we can determine using (2.8), the relationship between the end state of the wave $u_\infty = u_3$, and the point along T_{off} where the jump occurs: $(u, w_+) = (u_3, c^2/2u_3)$.

For $u > 0$, $w < 0$, there is a single w-nullcline, which trajectories cross from right to left, as well as the $\{u = 0\}$-nullcline, along which trajectories travel upwards. Between the u-axis and this negative w-nullcline, solution trajectories are monotonically decreasing in u and increasing in w. Below the negative w-nullcline solution trajectories are monotonically decreasing in both u and w. Consequently, jumps landing on S_a with $w < 0$ connect to a
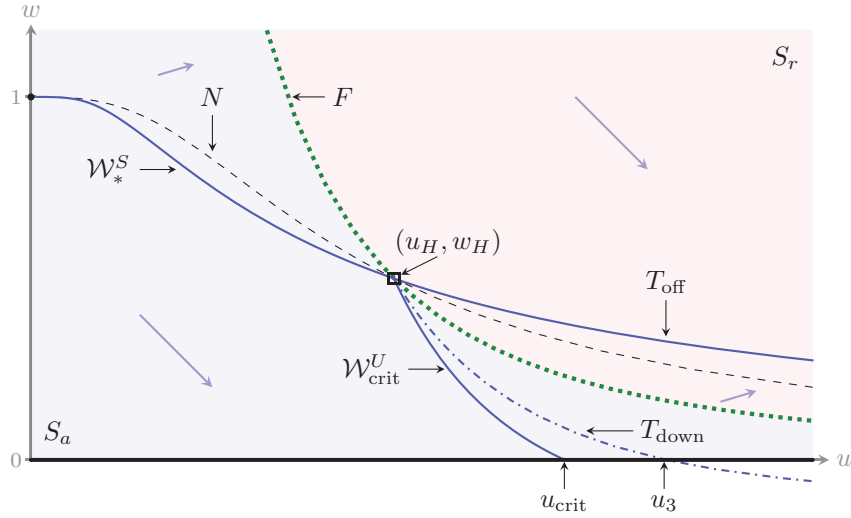
Figure 2.4: An illustration of the important curves and points in the phase plane of the reduced problem. The blue shaded region corresponds to S_a and the red shaded region to S_r. The blue arrows are indicative of the sign of the derivative (2.14), and consequently the monotonic decrease or increase of solution trajectories in the respective regions.

stable steady state, thus completing the heteroclinic orbit. These connections represent Type IV waves, and akin to the Type II waves, consist of the three components $\Gamma = \gamma_c \cup \gamma_f \cup \gamma_s$, but where $w < 0$ along γ_s. ■

The Type II, III and IV waves correspond to travelling wave solutions with a shock, with the Type II and III waves together equivalent to the Type 2 waves in [24]. Examples of Type II, III and IV waves with the corresponding phase trajectories are shown in Figures 2.5b, 2.5c and 2.5d, respectively.

2.4. Uniqueness of heteroclinic orbits. We are also interested in the uniqueness of the singular heteroclinic orbits constructed in §2.2 and §2.3. For a travelling wave solution to be unique we require that for fixed c and u_∞, only one heteroclinic orbit exists connecting the unstable steady state $(0, 1)$ to the stable steady state $(u_\infty, 0)$.

Lemma 2.8. *The singular heteroclinic orbits representing Type I, II, III and IV waves are unique.*

Proof. The uniqueness of the heteroclinic orbits constructed as Type I, II, III and IV waves follows from the following lemmas. The first concerns the transversality of the vector field (2.14) and T_{down}. If the vector field were tangent to T_{down} at any point, we would observe non-unique solutions.

Lemma 2.9. *The vector field (2.14) has a transverse intersection with T_{down}.*

Proof. We know that along T_{down} the vector field satisfies (2.14) with $w = w_-(u)$. Furthermore, since we are only considering $u > u_H$ and $w < w_H$, we can relate w_- to w_+ using (2.8). Therefore, demonstrating the transversality of the intersection between the vector field
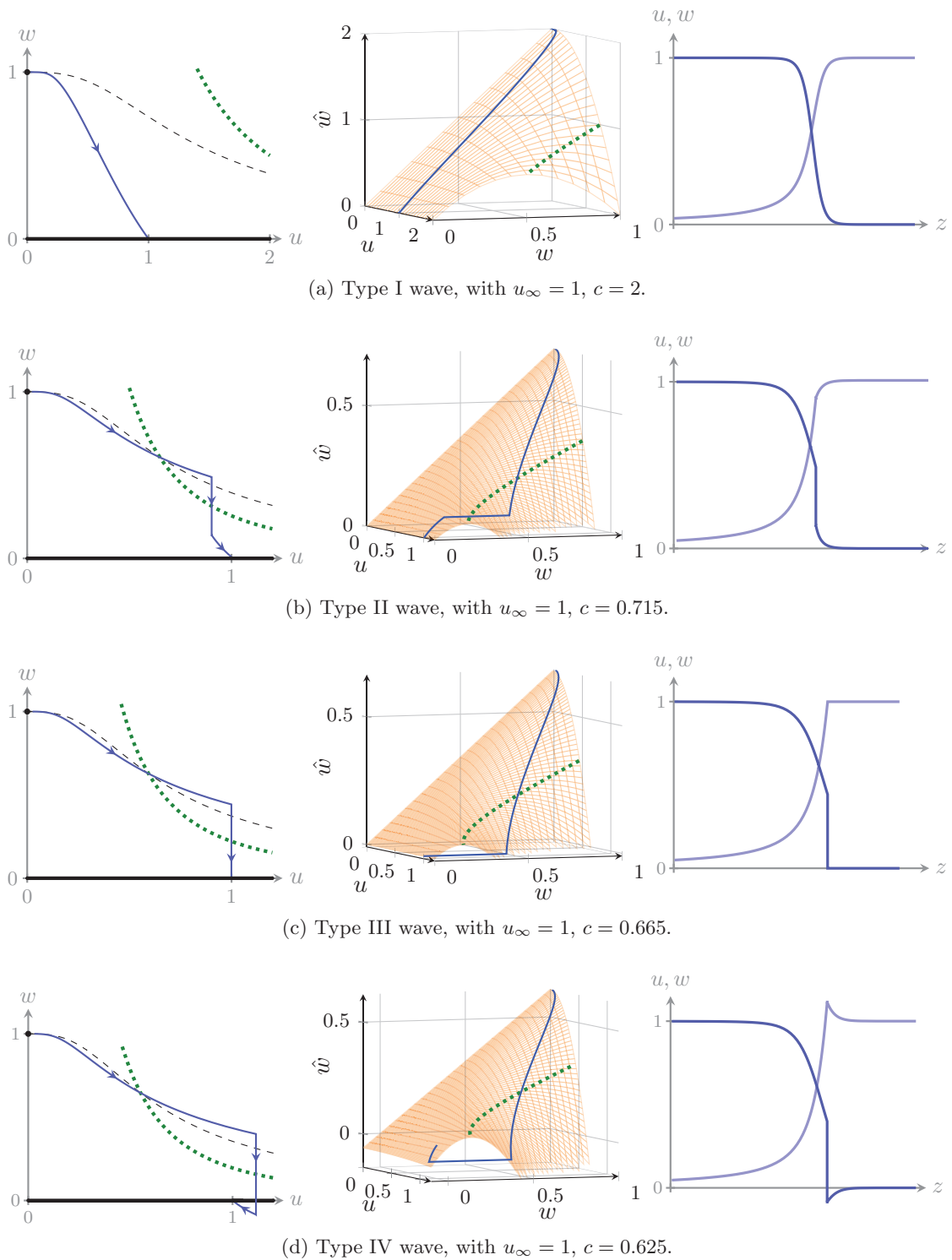
(a) Type I wave, with $u_\infty = 1$, $c = 2$.

(b) Type II wave, with $u_\infty = 1$, $c = 0.715$.

(c) Type III wave, with $u_\infty = 1$, $c = 0.665$.

(d) Type IV wave, with $u_\infty = 1$, $c = 0.625$.

Figure 2.5: Example solutions for the four types of waves described in §2.2 and §2.3. The first columns shows the singular heteroclinic orbit in the phase plane of the reduced vector field, with the vertical lines representing the diversion along a fast fibre. The second column is the same orbit plotted onto the critical manifold S. In these figures, the diversion along a fast fibre is more easily seen, as we can explicity see the trajectory leaving S. The third column shows the corresponding wave shape for each orbit. The darker line is the w solution and the lighter one the u solution. Note that the singular heteroclinic orbits are constructed numerically by solving the desingularised system (2.12) using MATLAB's inbuilt ODE solvers and then manually inserting the jump at the appropriate location.

(2.14) and T_{down} requires showing that

$$\frac{\mathrm{d}T_{\text{down}}}{\mathrm{d}u} - \frac{\mathrm{d}w}{\mathrm{d}u}\bigg|_{w=w_-=2F(u)-w_+} \neq 0.$$

This defines the transversality condition, where the former derivative denotes the slope of T_{down} and the latter the vector field (2.14) along it. Recalling that $w_-(u) = T_{\text{down}}$ (and $w_+(u) = T_{\text{off}}$), we again use (2.8) to rewrite the slope of T_{down} as

$$\frac{\mathrm{d}T_{\text{down}}}{\mathrm{d}u} = \frac{\mathrm{d}w_-(u)}{\mathrm{d}u} = 2\frac{\mathrm{d}F(u)}{\mathrm{d}u} - \frac{\mathrm{d}w_+(u)}{\mathrm{d}u}. \tag{2.15}$$

Along $w_+(u) = T_{\text{off}}$ the vector field is tangent to T_{off} as this is a solution trajectory. Thus, the final derivative in (2.15) is written simply as the vector field (2.14) evaluated at $w = w_+$, and we rewrite the transversality condition as

$$\frac{\mathrm{d}T_{\text{down}}}{\mathrm{d}u} - \frac{\mathrm{d}w}{\mathrm{d}u}\bigg|_{w=w_-} = 2\frac{\mathrm{d}F(u)}{\mathrm{d}u} - \frac{\mathrm{d}w}{\mathrm{d}u}\bigg|_{w=w_+} - \frac{\mathrm{d}w}{\mathrm{d}u}\bigg|_{w=2F(u)-w_+}.$$

Recalling from (1.4) that $F(u) = c^2/2u^2$, we evaluate the derivatives on the right hand side of the above expression by explicitly differentiating $F(u)$, and substituting $w = w_+$ and $w = 2F(u) - w_+ = c^2/u^2 - w_+$ into (2.14), respectively to give

$$\frac{\mathrm{d}T_{\text{down}}}{\mathrm{d}u} - \frac{\mathrm{d}w}{\mathrm{d}u}\bigg|_{w=w_-} = -\frac{2c^2}{u^3} + \frac{c^2(1-w_+)-2u^3w_+^2}{u^2(c^2-2u^2w_+)} + \frac{c^2(1-(c^2/u^2-w_+))-2u^3(c^2/u^2-w_+)^2}{u^2(c^2-2u^2(c^2/u^2-w_+))}$$

$$= \frac{c^2}{u^4} > 0 \quad \text{for } c, u \neq 0.$$

Thus T_{down} does not lie tangent to, but rather will always be less steep than, the vector field at any point. ■

 The second opportunity for non-unique solutions to arise is if $\mathcal{W}^U_{\text{crit}} \geq T_{\text{down}}$ at any point. Consider the regime depicted in Figure 2.6b, or in fact any regime where $\mathcal{W}^U_{\text{crit}} \geq T_{\text{down}}$. Under this regime we can identify multiple pairs of solutions (one with and one without a shock) that connect $(0,1)$ to the same $(u_\infty, 0)$ end state. One such example is drawn in Figure 2.6b. Here, to connect $(0,1)$ and $(u_{\text{crit}}, 0)$ the solution can either follow $\mathcal{W}^S_*$ then $\mathcal{W}^U_{\text{crit}}$, or $\mathcal{W}^S_*$ then T_{off} until a jump is made to the intersection point between $\mathcal{W}^U_{\text{crit}}$ and T_{down}, after which the solutions continues to $(u_{\text{crit}}, 0)$.

 Lemma 2.10. *For all $u > u_H$, $T_{\text{down}}(u) > \mathcal{W}^U_{\text{crit}}(u)$.*

 Proof. From Lemma 2.9, we know that for $u > u_H$, $\mathcal{W}^U_{\text{crit}}$ can only intersect T_{down} from top to bottom. That is, if an intersection occurs at $(u,w) = (u^*, w^*)$, $\mathcal{W}^U_{\text{crit}}(u) > T_{\text{down}}(u)$ for $u < u^*$ and $\mathcal{W}^U_{\text{crit}}(u) < T_{\text{down}}(u)$ for $u > u^*$. If the intersection were to occur in the opposite direction (as depicted in Figure 2.6b), the vector field at the point of intersection would be less steep than the instantaneous slope of T_{down}, which is in contradiction to Lemma 2.9. (They also cannot touch without intersecting as this would result in their gradients being equal at that point.) Therefore, if $\mathcal{W}^U_{\text{crit}}$ is greater than T_{down} at any point, it must be initially, as the two curves leave the canard point.
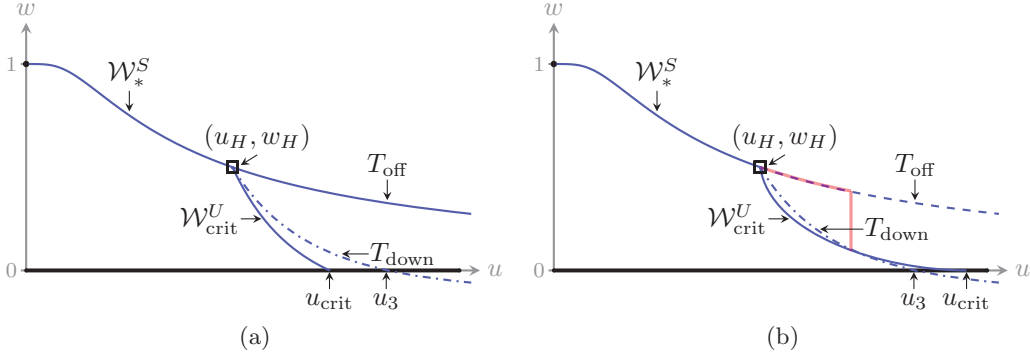
Figure 2.6: An illustration of the possibility of non-unique solutions if $\mathcal{W}^U_{\text{crit}} > T_{\text{down}}$ for any $u > u_H$. The left hand figure displays the actual location of the curves $\mathcal{W}^U_{\text{crit}}$ and T_{down}, showing no intersection and $T_{\text{down}} > \mathcal{W}^U_{\text{crit}}$ for all $u > u_H$. The right hand figure gives example locations of the curves $\mathcal{W}^U_{\text{crit}}$ and T_{down}, that lead to non-unique solutions. In this case, there are two possible connections to u_{crit}. Firstly, by following $\mathcal{W}^S_*$ and then $\mathcal{W}^U_{\text{crit}}$; secondly, by following $\mathcal{W}^S_*$, then T_{off} until switching onto a fast fibre as shown in red, and finally following $\mathcal{W}^U_{\text{crit}}$ to the steady state $(u_{\text{crit}}, 0)$. Note that the right hand figure violates the transversality condition of Lemma 2.9.

Consider a linearisation around the canard point, where we are interested in the difference in slope (at a linear level) of T_{down} and $\mathcal{W}^U_{\text{crit}}$:

$$\frac{\mathrm{d}T_{\text{down}}}{\mathrm{d}u} - \frac{\mathrm{d}\mathcal{W}^U_{\text{crit}}}{\mathrm{d}u}.$$

The eigenvectors of the canard point are

$$\boldsymbol{\psi}^\pm = (f^\pm(c), -1),$$

where

$$f^\pm(c) = \frac{c^2(c+B)^4}{64(c^2+cB+1) \pm 2(c+B)^2\sqrt{16+24cB-48c^2+6c^3B-6c^4}},$$

with $B = \sqrt{c^2+8}$. In this case, $\boldsymbol{\psi}^+$ corresponds to the direction of $\mathcal{W}^U_{\text{crit}}$ and $\boldsymbol{\psi}^-$ to T_{off}. Hence, by taking the gradient of the eigenvectors and using (2.15), we approximate the difference in slopes of T_{down} and $\mathcal{W}^U_{\text{crit}}$ near the canard point by

$$\frac{\mathrm{d}T_{\text{down}}}{\mathrm{d}u} - \frac{\mathrm{d}\mathcal{W}^U_{\text{crit}}}{\mathrm{d}u} \approx \frac{\mathrm{d}T_{\text{down}}}{\mathrm{d}u} + \frac{1}{f^+(c)} = 2\left.\frac{\mathrm{d}F(u)}{\mathrm{d}u}\right|_{u=u_H} + \frac{1}{f^-(c)} + \frac{1}{f^+(c)}. \tag{2.16}$$

Consider only the sum

$$\frac{1}{f^-(c)} + \frac{1}{f^+(c)} = \frac{f^+(c) + f^-(c)}{f^+(c)f^-(c)},$$

where

$$f^{\pm}(c) = \frac{\alpha}{\beta \pm \gamma},$$

with

$$\alpha = c^2(c+B)^4, \quad \beta = 64(c^2 + cB + 1), \quad \gamma = 2(c+B)^2\sqrt{16 + 24cB - 48c^2 + 6c^3B - 6c^4}.$$

Then,

$$\frac{f^+(c) + f^-(c)}{f^+(c)f^-(c)} = \left(\frac{2\alpha\beta}{\beta^2 - \gamma^2}\right) \Big/ \left(\frac{\alpha^2}{\beta^2 - \gamma^2}\right) = \frac{2\beta}{\alpha},$$

and we can simplify (2.16) to

$$\frac{dT_{\text{down}}}{du} + \frac{1}{f^+(c)} = -\frac{2c^2}{u_H^3} + \frac{2\beta}{\alpha} = -\frac{128}{c(c+B)^3} + \frac{128(c^2 + cB + 1)}{c^2(c+B)^4} = \frac{128}{c^2(c+B)^4},$$

which is positive for all $c \neq 0$. Therefore, we can say that near the canard point T_{down} lies above $\mathcal{W}_{\text{crit}}^U$, which together with Lemma 2.9, implies that in fact $T_{\text{down}} > \mathcal{W}_{\text{crit}}^U$ for all $u > u_H$. ∎

The vector fields of the layer problem (2.6) and the desingularised system (2.12) are continuous, and sufficiently smooth to ensure uniqueness within the individual problems. The existence of the canard point in the reduced problem provides a unique trajectory that connects $(0,1)$ to (u_H, w_H). This, together with the above results, guarantees the uniqueness of the heteroclinic orbits representing Type I, II, III and IV waves. ∎

An implication of Lemma 2.10 is that $u_3 > u_{\text{crit}}$. This implies that for fixed c, as u_∞ is increased (or similarly for fixed u_∞ and decreasing c) the singular heteroclinic orbits vary from representing Type I, to Type II, Type III and Type IV waves, in that order, as depicted in Figure 2.7b. In particular, for fixed c, Type I waves exist for $0 < u_\infty \leq u_{\text{crit}}$, Type II waves for $u_{\text{crit}} < u_\infty < u_3$, Type III waves for $u_\infty = u_3$, and Type IV waves for $u_3 < u_\infty < u_{\text{upper}}$, with $u_{\text{upper}} \in (u_3, \infty]$. Note that these results can also be expressed in terms of ranges of c, for fixed u_∞. A summary of where in the phase plane the different wave types are observed is given in Figure 2.7a.

2.5. Persistence of solutions for $0 < \varepsilon \ll 1$**.** *Proof.* [Proof of Theorem 2.1] Having constructed travelling wave solutions in the singular limit $\varepsilon \to 0$, we now show that these singular limit solutions persist as nearby solutions of the full problem (1.6) for sufficiently small $0 < \varepsilon \ll 1$, as in [39]. Firstly, we note that the end states of the waves $(0,1)$ and $(u_\infty, 0)$, which are the background states of (1.6), do not depend on ε and so remain unchanged for $\varepsilon > 0$.

The existence of Type I waves for $\varepsilon > 0$ follows from Fenichel theory alone [7]. Away from the fold curve, the normally hyperbolic manifolds S_a and S_r deform smoothly to locally invariant manifolds $S_{a,\varepsilon}$ and $S_{r,\varepsilon}$ respectively, and the slow flow on these manifolds is a smooth, $\mathcal{O}(\varepsilon)$ perturbation of the flow on S. Hence, the singular Type I waves Γ established in Lemma 2.5 will perturb to nearby Type I waves Γ_ε of the full system (1.6), connecting $(1,0)$ to $(u_\infty, 0)$. Note that since u_∞ is a free parameter, we in fact have a family of possible end states. Consequently, for a given singular heteroclinic orbit Γ connecting to a particular end
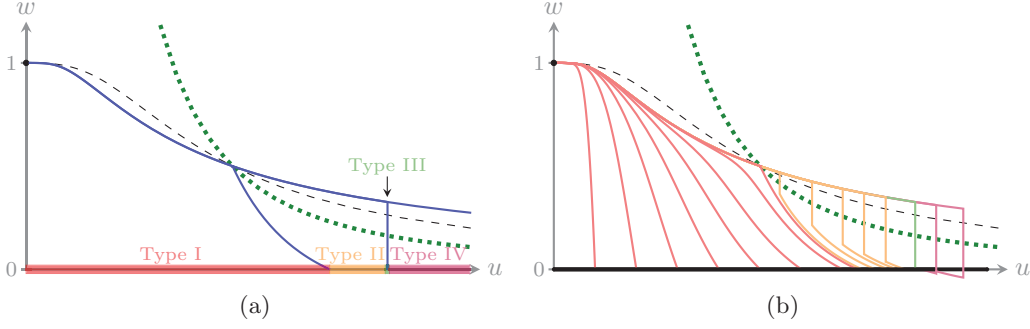
Figure 2.7: An illustration of the different types of waves observed as u_∞ is varied, for fixed $c = 1$. The left hand figure shows a schematic of the regions of the phase plane of the reduced problem in which the different wave types are observed. The right hand figure demonstrates the smooth transition between the wave types. Note that this smooth transition is also observed if u_∞ is fixed and c varied.

state $(u_\infty, 0)$ with wavespeed c, Γ_ε will connect to this end state with a nearby wavespeed $c(\varepsilon)$ for $\varepsilon > 0$, with $c(0) = c$. Equivalently, with the wavespeed fixed, the perturbed heteroclinic orbit Γ_ε connects to a nearby end state $(u_\infty(\varepsilon), 0)$ for $\varepsilon > 0$, with $u_\infty(0) = u_\infty$.

The existence of Type II–IV waves for $\varepsilon > 0$ follows from a combination of Fenichel theory, canard theory, and the transversality condition in Lemma 2.9. We first focus on the slow segments γ_c and γ_s of Γ defined in Lemmas 2.6 and 2.7. As mentioned above, away from the fold curve, S_a and S_r deform smoothly to locally invariant manifolds $S_{a,\varepsilon}$ and $S_{r,\varepsilon}$, and the slow flow on these manifolds is a smooth, $\mathcal{O}(\varepsilon)$ perturbation of the flow on S. Hence, the segment γ_s perturbs smoothly to γ_s^ε on $S_{a,\varepsilon}$ connecting to the end state $(u_\infty, 0)$. The persistence of the segment γ_c relies on canard theory [17, 33, 38] since normal hyperbolicity is lost near the fold. Canard theory guarantees the existence of a maximal folded saddle canard γ_c^ε in the full system. Geometrically speaking, the stable and unstable slow manifolds ($S_{a,\varepsilon}$ and $S_{r,\varepsilon}$) intersect transversally near the folded saddle singularity for $\varepsilon > 0$ within the three-dimensional centre manifold corresponding to the two slow and the non-hyperbolic fast direction; see [5] and [39] for details. This transverse intersection defines the so called *maximal canard*, and a family of canard solutions nearby, tracing the maximal canard exponentially close.

Next, we focus on the fast dynamics. The normally hyperbolic branch S_a has an associated local stable manifold $\mathcal{W}^S(S_a) = \cup_{p \in S_a} \mathcal{W}^S(p)$ (stable layer fibration) and the normally hyperbolic branch S_r has an associated local unstable manifold $\mathcal{W}^U(S_r) = \cup_{p \in S_r} \mathcal{W}^U(p)$ (unstable layer fibration). The points $p \in S_{a/r}$ are called *base points* of the fast fibres. Fenichel theory [7] implies that these local stable and unstable manifolds (fibrations) perturb smoothly to $\mathcal{O}(\varepsilon)$-close local stable and unstable fibrations $\mathcal{W}^S(S_{a,\varepsilon})$ and $\mathcal{W}^U(S_{r,\varepsilon})$ with base points $p_\varepsilon \in S_{a/r,\varepsilon}$. Recall that a fast segment γ_f connects the base points $w_+ = T_{\text{off}}(u) \in S_r$ and $w_- = T_{\text{down}}(u) \in S_a$ with $u = u_f$. Since the layer fibre intersection of $\mathcal{W}^U(T_{\text{off}}) \subset \mathcal{W}^U(S_r)$ and $\mathcal{W}^S(T_{\text{down}}) \subset \mathcal{W}^S(S_a)$ is transverse, it will persist for $0 < \varepsilon \ll 1$. The transversality condition

in Lemma 2.9 ensures that the two slow solution segments γ_c^ε and γ_s^ε intersect transversally (projected along fast fibres onto $S_{a,\varepsilon}$). This unique intersection point identifies the base point location $u_f(\varepsilon)$ for $\varepsilon > 0$ of the fibre intersection $\gamma_{f,\varepsilon}$ uniquely. Note that $\gamma_{f,\varepsilon}$ is not a solution of the full system (while γ_f is a solution of the layer problem).

Finally, recall that the end state $(u_U, w_U) \in S_{a,\varepsilon}$ is repelling for $u \geq 0$. This end state can only be approached in backward z by solutions that are in $S_{a,\varepsilon}$ (which is only unique up to exponentially small terms). Note that the attracting manifold $S_{a,\varepsilon}$ extended past the folded saddle singularity aligns with the unstable fibres of $S_{r,\varepsilon}$. We just showed that the unstable fibration of $S_{r,\varepsilon}$ along γ_c^ε has a unique fibre intersection. Hence, if we start on this fibre we will approach the travelling wave end states in forward and backward z, and the singular Type II and Type IV waves Γ established in Lemmas 2.6 and 2.7 will perturb to nearby Type II and Type IV waves Γ_ε of the full system (1.6), connecting $(1,0)$ to $(u_\infty, 0)$ with nearby $c = c(\varepsilon)$. The above argument also holds for Type III waves, but without tracing backwards on $S_{r,\varepsilon}$.

■

3. Numerical analysis of asymptotic wavespeed.
In the previous section we used geometric singular perturbation theory to prove the existence and uniqueness of travelling wave solutions to (1.6), based on the analysis of the corresponding ODE system. When studying the ODE system, the wavespeed acts as an input parameter. However, in reality, the wavespeed is an output of the PDE system. The existence and uniqueness of travelling wave solutions provides no information about the stability of the solutions, in particular which wavespeed will be observed for a given initial condition. In this section, we investigate the observed wavespeeds of travelling wave solutions, numerically.

3.1. Estimating the wavespeed.
The model (1.6) under consideration is

$$u_t = -u^2 w + \varepsilon u_{xx},$$
$$w_t = w(1 - w) - (u_x w)_x + \varepsilon w_{xx}.$$

Linearising the desingularised system (2.12) (which arises from (1.6)) around $(u_\infty, 0)$ provides us with an approximation of the solution near $(u_\infty, 0)$:

$$\begin{pmatrix} u \\ w \end{pmatrix} = \begin{pmatrix} u_\infty \\ 0 \end{pmatrix} + A \begin{pmatrix} -u_\infty^2 \\ 1 \end{pmatrix} e^{-c\bar{z}},$$

where A is an appropriate integration constant. Furthermore, near $(u_\infty, 0)$, $\bar{z}$ is approximately z/c^2 so we have

$$\begin{pmatrix} u \\ w \end{pmatrix} = \begin{pmatrix} u_\infty \\ 0 \end{pmatrix} + A \begin{pmatrix} -u_\infty^2 \\ 1 \end{pmatrix} e^{-z/c}. \tag{3.1}$$

Consequently, we make the ansatz that the leading edges of the solutions behave like

$$u(x,t) = u_\infty - u_\infty^2 A e^{-\xi(x-ct)} = u_\infty(1 - u_\infty w(x,t)),$$
$$w(x,t) = A e^{-\xi(x-ct)}, \tag{3.2}$$

for asymptotically large x, with $\xi, A > 0$, and evolve from initial conditions with equivalent asymptotic behaviour. Substituting (3.2) into (1.6) gives

$$-\xi c u_\infty^2 w(x,t) = -(u_\infty - u_\infty^2 w(x,t))^2 w(x,t) - \varepsilon \xi^2 u_\infty^2 w(x,t),$$
$$\xi c w(x,t) = w(x,t)(1 - w(x,t)) + 2\xi^2 u_\infty^2 w^2(x,t) + \varepsilon \xi^2 w(x,t).$$

Since $w \to 0$ as $x \to \infty$, we neglect the $\mathcal{O}(w^2)$-terms to obtain the dispersion relation for both equations:

$$\xi c = 1 + \varepsilon \xi^2 \quad \text{or} \quad c = \varepsilon \xi + \frac{1}{\xi}.$$

This dispersion relation is equivalent to that of the Fisher–KPP equation. Thus, applying the argument in [21, 26], we infer that solutions evolving from initial conditions with asymptotic behaviour equivalent to (3.2) will have wavespeeds:

$$c = \begin{cases} \frac{1}{\xi} + \varepsilon \xi, & \text{if } \xi < \frac{1}{\sqrt{\varepsilon}}, \\ 2\sqrt{\varepsilon}, & \text{if } \xi \geq \frac{1}{\sqrt{\varepsilon}}. \end{cases} \tag{3.3}$$

For $\varepsilon = 0$, (3.3) suggests a wavespeed of $c = 1/\xi$ for all ξ. This has been numerically verified for Type I and II waves [24]. However, minimum wavespeed waves with semi-compact support (Type III waves) were also observed in [24], where the speed of these waves was much greater than the expected value of zero and evolved from initial conditions with various, finite values of ξ. This result is in contradiction to (3.3), however is not unexpected since the analysis is not valid for Type III waves. Initial conditions with semi-compact support also evolved to the minimum wavespeed, Type III wave [24]. No numerical experiments were carried out for $\varepsilon > 0$ in [24] as their model did not include diffusion.

3.2. Numerical results for $\varepsilon > 0$. We investigate the validity of (3.3) for $\varepsilon > 0$. To solve (1.6) we employ a numerical scheme that uses the finite volume method for the spatial discretisation, with a third order upwinding scheme for the advection term and linearisation in time of the non-linear source term $w(1 - w)$, and a Crank–Nicolson timestepping scheme. We choose initial conditions with appropriate asymptotic behaviour for large x:

$$u(x,0) = u_\infty, \quad w(x,0) = \begin{cases} 1 & \text{if } x \leq x_0, \\ e^{-\xi(x-x_0)} & \text{if } x > x_0, \end{cases} \tag{3.4}$$

where $x_0 = L/5$ with L the length of the domain.

Figure 3.1 shows a comparison between (3.3) (solid lines) and the numerically measured wavespeeds (markers), for various values of ε ($\varepsilon = 0, 0.05, 0.1, \ldots, 0.5$) with fixed $u_\infty = 1$. We observe that the markers appear to lie on the solid lines up to a critical value of ξ. Beyond this, (3.3) suggests the curves should flatten out to $2\sqrt{\varepsilon}$, the expected minimum wavespeed. However, this is only true for moderate values of ε, in the case where $u_\infty = 1$ approximately $\varepsilon \geq 0.3$. For smaller values of ε, the transition to the minimum wavespeed occurs for smaller values of ξ and larger values of c than suggested by (3.3).

For wavespeeds above the minimum wavespeed, both Type I and Type II waves are observed numerically; Type I waves for smaller values of ξ (corresponding to faster wavespeeds),
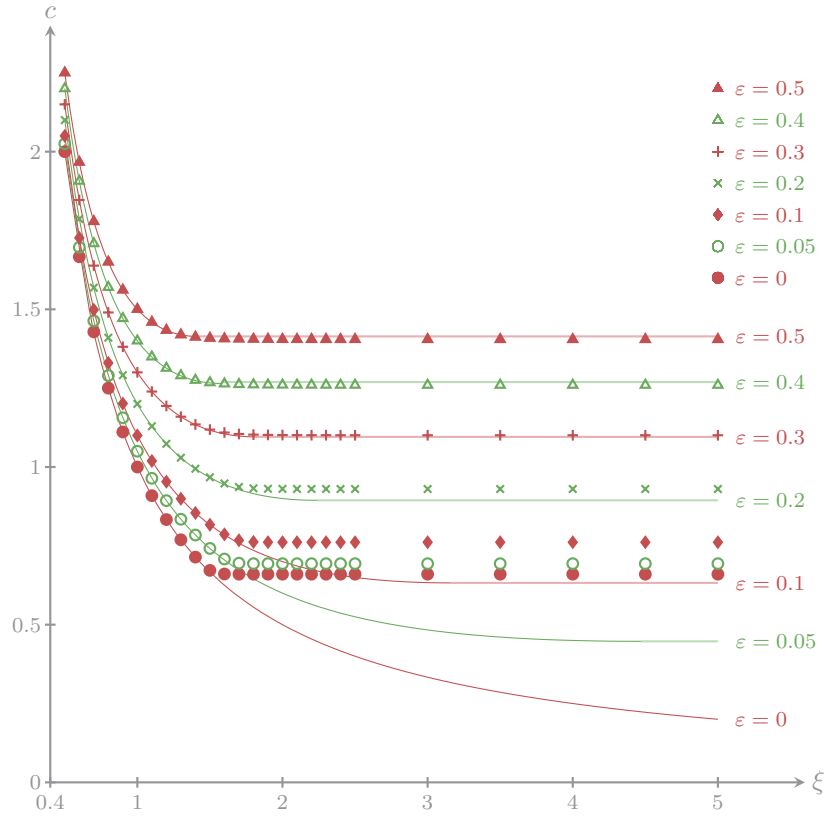
Figure 3.1: A plot of the numerically measured wavespeeds (markers) against (3.3) (solid lines) for various values of ξ and ε. The colours of the curves and markers are alternated purely as a visual aid, they do not represent anything mathematically significant.

and Type II waves for larger values of ξ (corresponding to slower wavespeeds). However, as seen (or rather not seen) in Figure 3.1, there is no distinguishing feature visible in the data to suggest a transition from Type I to Type II waves. This is because the transition point is determined by u_∞; in particular, the value of u_∞ corresponding to $u_\infty = u_{\mathrm{crit}}(c, \varepsilon)$ for the chosen values of ξ, ε, and consequently c.

For wavespeeds equal to the minimum wavespeed, only Type III waves are observed. Since this minimum wavespeed is greater than that suggested by (3.3) from the linear analysis, the numerical results indicate that the Type III wave is a *pushed front*, in contrast to the Type I and II waves which are *pulled fronts* [35]. We still require an expression for the minimum wavespeed. No Type IV waves were observed numerically to evolve from initial conditions of the kind used here. Furthermore, initial conditions similar to the Type IV wave in Figure 2.5d evolved to a Type III wave.

Figure 3.2 shows the relationship between the minimum wavespeed and u_3. The solid, blue curve is numerical data obtained from the ODE solver for (2.12). The black, dashed curve represents the power series approximation between c and u_3 given in [24], assuming small c.

(Note that [24] also provides an approximation assuming large c, which compares well against our numerical results, but is not shown here.) The remaining curves are plots of numerical data obtained from the PDE solver for various values of ε ($\varepsilon = 0, 0.02, \ldots, 0.1, 0.2, \ldots, 0.5$), with c increasing as ε increases.
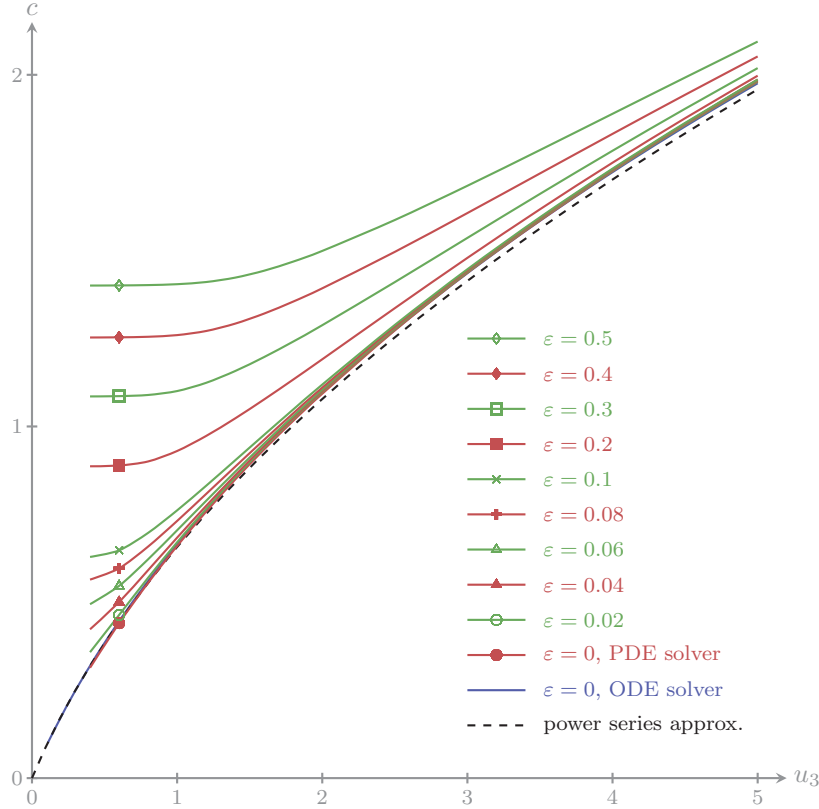

Figure 3.2: The minimum wavespeed as a function of u_∞. Since the minimum wavespeed wave corresponds to a Type III wave, $u_\infty = u_3$. The solid, blue curve is data obtained from the numerical solution of the ODE system (2.12), and so is for $\varepsilon = 0$. The dashed, black curve is a power series approximation between u_3 and c for $\varepsilon = 0$ given in [24]. The remaining curves show data from the numerical solution of the PDE system (1.6) for $\varepsilon = (0, 0.02, \ldots, 0.1, 0.2, \ldots, 0.5)$, as labelled. The colours of these curves are alternated purely a visual aid, and do not represent anything mathematically significant.

A first observation is that the data from the PDE and ODE solvers for $\varepsilon = 0$ compare well. They also compare well with the power series approximation suggested in [24], which is only for $\varepsilon = 0$. The results suggest that the minimum wavespeed depends not only on ε as suggested by (3.3), but also u_∞ or u_3. The power series solution in [24] suggests a quadratic relationship for $\varepsilon = 0$, however we do not have an approximation for $c = c(u_3, \varepsilon)$ for $\varepsilon \neq 0$.

For $\varepsilon \neq 0$, the most notable feature of the plots is the flattening out of the curves for small u_3. This indicates that for sufficiently large ε and sufficiently small u_3, the dependence of the

minimum wavespeed on u_3 is removed, that is, it only depends on ε: $c = c(\varepsilon)$. However, the curves suggest that independent of the size of ε, for sufficiently large values of u_3, the minimum wavespeed will still depend on u_3, and the power series provides a reasonable approximation. That is, as $u_3 \to \infty$, $c(u_3, \varepsilon) \approx c(u_3, 0) \sim \sqrt{u_3}$.

3.3. Numerical results for $\varepsilon = 0$**.** An interesting result from the numerical solutions of the ODE system, is the relationship between the jump length of Type II, III and IV waves and u_∞. The jump length is measured as $w_+ - w_-$, with results for various wavespeeds depicted in Figure 3.3. In particular, Figure 3.3a illustrates the relationship between the jump length of a particular wave and its end state u_∞, and Figure 3.3b, the relationship between the jump length and the value of u where the jump occurs. As expected, at the onset of Type II waves the jump length is zero, and then increases as u_∞ or u increases. The jump length corresponding to the Type III wave is marked with an $\times$. As u_∞ or u increases further, the jump length reaches a maximum and starts to decrease once more. This implies that there is a turning point in the difference between the take-off curve $w = T_{\text{off}}(u)$ and the fold curve $w = F(u)$.

Furthermore, these numerical results suggest that for any given c, there is a maximum value of u_∞ for the existence of travelling waves as constructed in this article; that is, u_{upper} is finite. This is clearly seen in Figure 3.3a. However, although there appears to be a maximum value of u_∞, the u-location of the jump is not bounded. That is, as the jump length goes to zero, the jump location goes to infinity. This is demonstrated in Figure 3.3b. An example trajectory for the Type IV wave with a jump length close to zero is shown in Figure 3.3c. This illustrates the point that as the jump location moves closer to infinity, the jump size decreases, and that the corresponding end state of the wave u_∞, though also increasing, appears to be bounded.

Finally, as c is increased, Figures 3.3a and 3.3b indicate that the maximum jump length decreases, and approaches zero as $c \to \infty$. This is to be expected, since $(u_H, w_H) \to (\infty, 0)$ as $c \to \infty$, so all the solutions will be Type I and therefore not contain a jump.

4. Discussion. Thus far, we have proved the existence and uniqueness of travelling wave solutions to a model of malignant tumour invasion (1.6) for sufficiently small $0 \leq \varepsilon \ll 1$. The wavespeed of the travelling wave solutions that evolved from initial conditions (3.4) was also discussed. Other initial conditions for w were also considered that had the required asymptotic behaviour, but are not shown here. In all cases the resulting wavespeed was equivalent to that resulting from (3.4).

The proof of existence of travelling wave solutions to (1.6) was constructed using geometric singular perturbation theory. Accordingly, the solutions were constructed as heteroclinic orbits in the singular limit $\varepsilon \to 0$, and then extended to solutions of the full system (1.6) using Fenichel theory and the theory of canard solutions, assuming sufficiently small ε. These travelling wave solutions were classified as Type I, II, III or IV waves.

In [29], diffusion was neglected as it was assumed that it played a small role in the migration process. We have provided a rigorous proof of the travelling wave solutions for $\varepsilon = 0$ found numerically in [24], and furthermore, have shown that these solutions persist for small ε. Therefore, we can confirm that the effect of diffusion is in fact small.
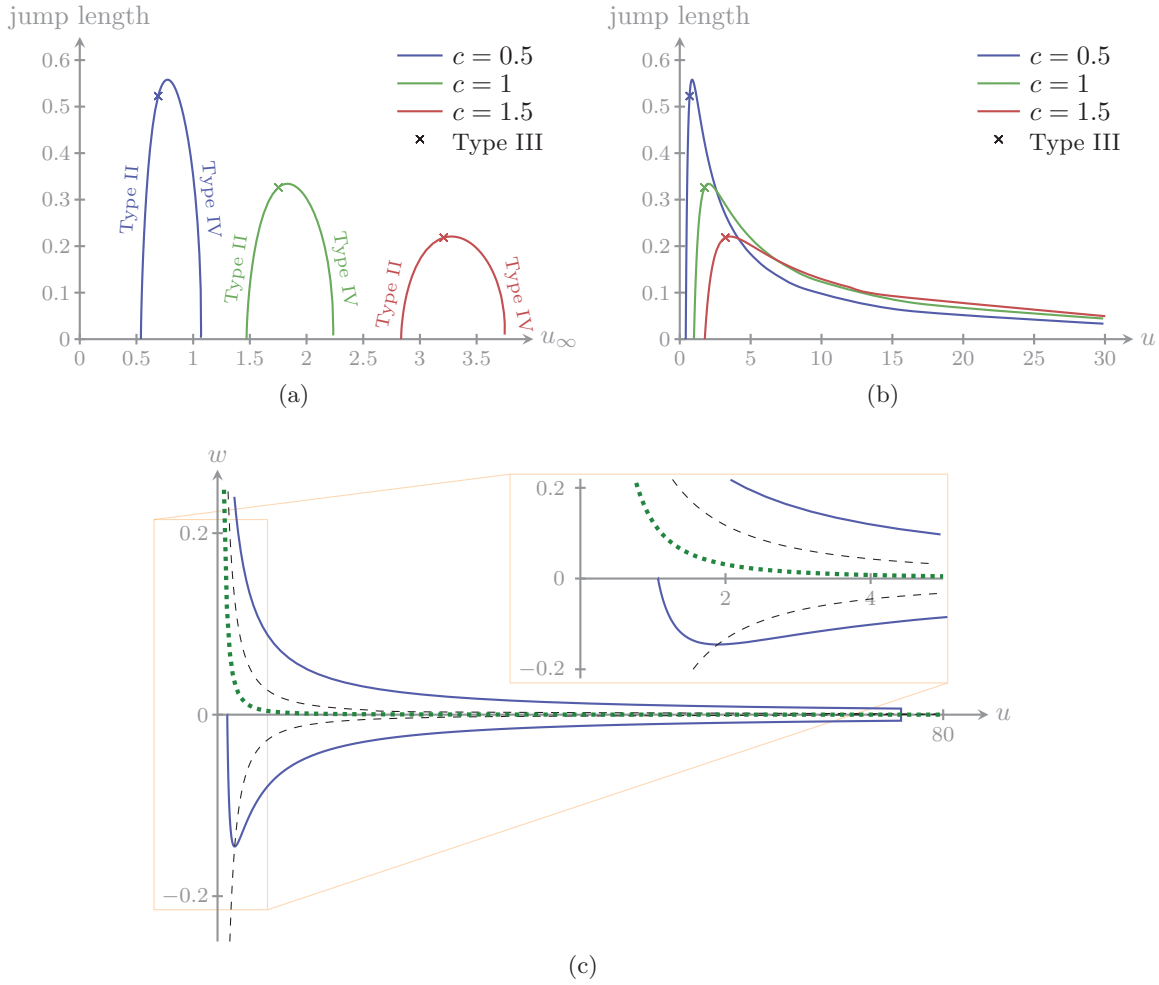
(a)

(b)

(c)

Figure 3.3: The first two plots show data from the numerical solutions of the ODE system (2.12) illustrating how the jump length varies with u_∞ and u, for various values of c (and $\varepsilon = 0$). The jump length corresponding to a Type III wave is marked with an $\times$. The corresponding value of u_∞ or u at this point is $u_\infty = u_3$. Before this (for smaller values of u_∞ or u) the waves are Type II waves, and after (for larger values of u_∞ or u) are Type IV waves. The third plot shows an example trajectory for a Type IV wave with jump length close to zero, with $c = 0.5$.

4.1. Protease. Recall that in §1.4 a third expression was neglected in (1.2) describing the density of protease ρ:

$$\frac{\partial \rho}{\partial t} = \frac{1}{\delta}(uw - \rho), \tag{4.1}$$

where $0 < \delta \ll 1$. This expression was neglected as it was assumed in [29] that the protease reaction occurred on a sufficiently fast time scale that the protease density could be considered to be at steady state to leading order. Subsequently we ask: which is smaller, the added

diffusivity ε in (1.6) or the inverse protease density rate parameter δ?

For our analysis we assume that $\delta = \mathcal{O}(\varepsilon^{\eta})$, where $\eta > 1$, such that $\delta \to 0$ faster than ε and the protease reaction can be neglected even when the diffusion is not. In [25], the authors consider the full system of three partial differential equations, (1.2) and (4.1). They suggest that travelling wave solutions are not observed for this model unless diffusion is added to the cell species w, with $\varepsilon = \mathcal{O}(\delta)$. Throughout the analysis, parameter regimes with both $\varepsilon > \delta$ and $\varepsilon < \delta$ are considered. The former regime gives rise to solutions that appear to be an $\mathcal{O}(\varepsilon)$ perturbation of the solutions constructed in the singular limit, whereas the latter results in solutions that exhibit oscillations at the wave front. This suggests that our assumption that $\delta \to 0$ faster than ε is reasonable. Analysis of the full system (1.2) and (4.1) using the method employed here is the topic of future investigation, to explore the effect of the relative sizes of δ and ε.

REFERENCES

[1] E. BARBERA, C. CURRÒ, AND G. VALENTI, *A hyperbolic model for the effects of urbanization on air pollution*, Appl. Math. Model., 34 (2010), pp. 2192–2202.

[2] M. BECK, A. DOELMAN, AND T.J. KAPER, *A geometric construction of traveling waves in a bioremediation model*, J. Nonlinear Sci., 16 (2006), pp. 329–349.

[3] E. BENOIT, J.L. CALLOT, F. DIENER, AND M. DIENER, *Chasse au canards*, Collect. Math., 31 (1981), pp. 37–119.

[4] N.F. BRITTON, *Reaction-Diffusion Equations and their Applications to Biology*, Academic Press, New York, 1986.

[5] M. BRØNS, M. KRUPA, AND M. WECHSELBERGER, *Mixed mode oscillations due to the generalized canard phenomenon*, Fields Inst. Commun., 49 (2006), pp. 39–63.

[6] A. DOELMAN, P. VAN HEIJSTER, AND T. KAPER, *Pulse dynamics in a three-component system: Existence analysis*, J. Dynam. Differential Equations, 21 (2009), pp. 73–115.

[7] N. FENICHEL, *Geometric singular perturbation theory for ordinary differential equations*, J. Differential Equations, 31 (1979), pp. 53–98.

[8] R.A. FISHER, *The wave of advance of advantageous genes*, Ann. Eugenics, 7 (1937), pp. 353–369.

[9] G. HEK, *Geometric singular perturbation theory in biological practice*, J. Math. Biol., 60 (2010), pp. 347–386.

[10] H. HOSHINO, *Traveling wave analysis for a mathematical model of malignant tumor invasion*, Analysis (Munich), 31 (2011), pp. 237–248.

[11] C.K.R.T. JONES, *Geometric singular perturbation theory*, in Dynamical Systems, vol. 1609, Springer Berlin / Heidelberg, 1995, pp. 44–118.

[12] D.W. JORDAN AND P. SMITH, *Nonlinear Ordinary Differential Equations*, Oxford University Press, 3 ed., 1999.

[13] T.J. KAPER, *An introduction to geometric methods and dynamical systems theory for singular perturbation problems*, in Proceedings of Symposia in Applied Mathematics, vol. 56, American Mathematical Society, 1999, pp. 85–131.

[14] E.F. KELLER AND L.A. SEGEL, *Model for chemotaxis*, J. Theoret. Biol., 30 (1971), pp. 225–234.

[15] ——, *Traveling bands of chemotactic bacteria: A theoretical analysis*, J. Theoret. Biol., 30 (1971), pp. 235–248.

[16] A. KOLMOGOROFF, I. PETROVSKY, AND N. PISCOUNOFF, *Étude do l'équation de la diffusion avec crois-*

sance de la quantité de matière et son application à un problème biologique, Moscow Univ. Math. Bull., 1 (1937), pp. 1–25.

[17] M. Krupa and P. Szmolyan, *Extending geometric singular perturbation theory to nonhyperbolic points—fold and canard points two dimensions*, SIAM J. Math. Anal., 33 (2001), pp. 286–314.

[18] K.A. Landman, G.J. Pettet, and D.F. Newgreen, *Chemotactic cellular migration: Smooth and discontinuous travelling wave solutions*, SIAM J. Appl. Math., 63 (2003), pp. 1666–1681.

[19] K.A. Landman, M.J. Simpson, and G.J. Pettet, *Tactically-driven nonmonotone travelling waves*, Phys. D, 237 (2008), pp. 678–691.

[20] K.A. Landman, M.J. Simpson, J.L. Slater, and D.F. Newgreen, *Diffusive and chemotactic cellular migration: Smooth and discontinuous travelling wave solutions*, SIAM J. Appl. Math., 65 (2005), pp. 1420–1442.

[21] D.A. Larson, *Transient bounds and time-asymptotic behavior of solutions to nonlinear equations of Fisher type*, SIAM J. Appl. Math., 34 (1978), pp. 93–103.

[22] B.P. Marchant and J. Norbury, *Discontinuous travelling wave solutions for certain hyperbolic systems*, IMA J. Appl. Math., 67 (2002), pp. 201–224.

[23] B.P. Marchant, J. Norbury, and H.M. Byrne, *Biphasic behaviour in malignant invasion*, Math. Med. Biol., 23 (2006), pp. 173–196.

[24] B.P. Marchant, J. Norbury, and A.J. Perumpanani, *Traveling shock waves arising in a model of malignant invasion*, SIAM J. Appl. Math., 60 (2000), pp. 463–476.

[25] B.P. Marchant, J. Norbury, and J.A. Sherratt, *Travelling wave solutions to a haptotaxis-dominated model of malignant invasion*, Nonlinearity, 14 (2001), pp. 1653–1671.

[26] H.P. McKean, *Application of Brownian motion to the equation of Kolmogorov-Petrovskii-Piskunov*, Comm. Pure Appl. Math., 28 (1975), pp. 323–331.

[27] J.D. Meiss, *Differential Dynamical Systems*, SIAM, 2007.

[28] J.D. Murray, *Mathematical Biology I: An Introduction*, Springer, 3rd ed., 2002.

[29] A.J. Perumpanani, J.A. Sherratt, J. Norbury, and H.M. Byrne, *A two parameter family of travelling waves with a singular barrier arising from the modelling of extracellular matrix mediated cellular invasion*, Phys. D, 126 (1999), pp. 145–159.

[30] G.J. Pettet, *Modelling wound healing angiogenesis and other chemotactically driven growth processes*, PhD thesis, University of Newcastle, 1996.

[31] G.J. Pettet, D.L.S McElwain, and J. Norbury, *Lotka-volterra equations with chemotaxis: Walls, barriers and travelling waves*, IMA J. Math. Appl. Med., 17 (2000), pp. 395–413.

[32] J. Smoller, *Shock Waves and Reaction-Diffusion Equations*, Springer Verlag, 2nd ed., 1994.

[33] P. Szmolyan and M. Wechselberger, *Canards in $\mathbb{R}^3$*, J. Differential Equations, 177 (2001), pp. 419–453.

[34] ——, *Relaxation oscillations in $\mathbb{R}^3$*, J. Differential Equations, 200 (2004), pp. 69–104.

[35] W. van Saarloos, *Front propagation into unstable states*, Phys. Rep., 386 (2003), pp. 29–222.

[36] M. Wechselberger, *Singularly perturbed folds and canards in $\mathbb{R}^3$*, PhD thesis, Vienna University of Technology, 1998.

[37] ——, *Existence and bifurcation of canards in $\mathbb{R}^3$ in the case of a folded node*, SIAM J. Appl. Dyn. Syst., 4 (2005), pp. 101–139.

[38] ——, *À propos de canards*, Trans. Amer. Math. Soc., 304 (2012), pp. 3289–3309.

[39] M. Wechselberger and G.J. Pettet, *Folds, canards and shocks in advection-reaction-diffusion models*, Nonlinearity, 23 (2010), pp. 1949–1969.